UCRL-16957

University of California

Ernest O. Lawrence Radiation Laboratory

DISLOCATION SUBSTRUCTURE IN SINGLE CRYSTALS OF HEXAGONAL Ag-Al ORIENTED FOR PRISMATIC SLIP

TWO-WEEK LOAN COPY

This is a Library Circulating Copy which may be borrowed for two weeks. For a personal retention copy, call Tech. Info. Division, Ext. 5545

DISCLAIMER

This document was prepared as an account of work sponsored by the United States Government. While this document is believed to contain correct information, neither the United States Government nor any agency thereof, nor the Regents of the University of California, nor any of their employees, makes any warranty, express or implied, or assumes any legal responsibility for the accuracy, completeness, or usefulness of any information, apparatus, product, or process disclosed, or represents that its use would not infringe privately owned rights. Reference herein to any specific commercial product, process, or service by its trade name, trademark, manufacturer, or otherwise, does not necessarily constitute or imply its endorsement, recommendation, or favoring by the United States Government or any agency thereof, or the Regents of the University of California. The views and opinions of authors expressed herein do not necessarily state or reflect those of the United States Government or any agency thereof or the Regents of the University of California.

Research and Development

UCRL-16957

UNIVERSITY OF CALIFORNIA

Lawrence Radiation Laboratory
Berkeley, California

AEC Contract No. W-7405-eng-48

DISLOCATION SUBSTRUCTURE IN SINGLE CRYSTALS OF HEXAGONAL Ag-Al ORIENTED FOR PRISMATIC SLIP

Paul R. Okamoto
(M.S. Thesis)

June 1966

DISLOCATION SUBSTRUCTURE IN SINGLE CRYSTALS
OF HEXAGONAL Ag-Al ORIENTED FOR PRISMATIC SLIP

Contents

ABSTRACT

I. Introduction 1

II. Experimental Procedure 4

A. Material 4

B. Specimen Preparation 4

C. Testing Procedures 4

D. Foil Orientation 5

III. Experimental Results 7

A. Stress-Strain Curves 7

B. Slip Line Patterns 8

C. The Effect of Temperature and Strain on the Dislocation Distribution 9

D. The Effect of Specimen Shape on Dislocation Distribution 14

E. Burgers Vector Determinations. 14

F. Dislocation Distribution Within a Slip Band. 16

G. Nature of the Prismatic Loops. 17

IV. Discussion. 20

A. Metastable Arrangements. 20

B. Formation of Slip Bands. 21

C. Formation of Loops and Helices 23

V. Conclusions. 27

ACKNOWLEDGMENTS 29

REFERENCES. 30

TABLE AND FIGURES. 32

DISLOCATION SUBSTRUCTURE IN SINGLE CRYSTALS OF HEXAGONAL Ag-Al ORIENTED FOR PRISMATIC SLIP

Paul R. Okamoto

Inorganic Materials Research Division, Lawrence Radiation Laboratory
Department of Mineral Technology, College of Engineering
University of California, Berkeley, California

June 1966

ABSTRACT

Single crystals of hexagonal Ag 33 at.% Al oriented for prismatic slip were deformed at various temperatures between 77°K and 500°K. The dislocation distribution was studied by transmission electron microscopy as a function of temperature and strain. Between 77°K and 400°K the predominant features of the dislocation distribution are broad slip bands containing a high density of perfect prismatic loops and long clusters of helical dislocations. Below 400°K the prominent features of dislocation distribution changes very little with increasing temperature. The effect of increasing total strain on the dislocation distribution is equivalent to a decrease in temperature. The slip bands and surface slip lines correlate with the serrations in the stress-strain curves. Between 400°K and 500°K the dislocation distribution becomes uniform and the prominent slip bands are not observed.

It is concluded that the dislocation distribution is in good agreement with the distribution expected from the theoretical strengthening mechanisms developed for this alloy. The high density of loops in the slip bands explains the anamolous behavior of the critical resolved shear stress reported by previous investigators.

I. INTRODUCTION

In recent years much effort has been directed towards a better understanding of the mechanical properties of the ζ intermediate phases of the noble metals. These phases are solid solutions which have the hexagonal close packed structure and generally occur after the primary α solid solutions in the phase diagrams. Interest in the ζ phases centers not only on their unusually high strength but also on their potentialities for studying the effects introduced by a change in crystal structure and higher solute concentrations on the various strengthening mechanisms developed for the α solid solutions.

In many respects the ζ Ag 33 at.% Al alloy and the $\langle 1\bar{2}10 \rangle$ $\{1\bar{1}00\}$ mode of slip is an ideal system for study from both an experimental and theoretical point of view. For example, since dislocations gliding on prismatic planes are not expected to be dissociated and in view of the similarity of the effective volumes for silver and aluminum atoms, possible ambiguities in interpretation arising from Suzuki and Cottrell locking will be minimized.

Furthermore, most ζ phases are stable over a wide composition range and form from the melt by a peritectic reaction. As a rule the two conditions lead to severe segregation problems when growing single crystals from the melt. However, in the ζ AgAl phase, the liquidus and solidus have practically the same solute composition, namely 33 at.% aluminum (see Fig. 1). Consequently, single crystals of Ag 33 at.% Al can be grown with very uniform composition.

In spite of the current interest in the ζ phases, transmission electron microscopy observations similar to those in deformed α solid solutions

have not been reported. The purpose of this investigation was to carry out such observations on single crystals of the ζ-Ag 33 at.% Al phase. In particular, the dislocation distribution produced during first order prismatic slip has been studied as a function of temperature and strain.

Previous work on this alloy by Mote et al.[1] showed that three rate controlling mechanisms can operate depending on test temperature. Their results together with the present data are shown in Fig. 2. Over region I the critical resolved shear stress (crss) decreases rapidly with temperature. More recent work by Rosen, et al.[2] has suggested that prismatic slip in this region is controlled by the nucleation and growth of kinks in dislocations lying in Peierls potential troughs. Over region II the crss is independent of temperature and the strain rate controlling mechanism has been ascribed to the destruction of short range order[1] by the Fisher mechanism. Finally, over region III, slip is again controlled by a thermally activated mechanism and the crss for prismatic slip drops below that for basal slip. A satisfactory theory for region III has not yet been established. However, on the basis of the work by Howard, et al.[3] the controlling mechanism has been tentatively ascribed to a diffusion controlled local disordering in the immediate vicinity of the dislocation.

In spite of the thorough investigation on the nature of prismatic slip there remains one anomalous experimental fact which has not been explained. In an attempt to ascertain whether disordering resulting from plastic deformation could be detected by a decrease in the crss in region II, Mote, et al.[1] prestrained their specimens at 77°K. After reloading and restraining in tension at 300°K, the crss was always identical with that obtained for well annealed crystals. This result is inconsistent

with the Fisher mechanism and implies either the absence of short range order or that very strong barriers to dislocations are formed on active slip planes forcing further slip to occur in undeformed regions of the crystals. Since X-ray diffraction data[4] on the local degree or order in this system has confirmed the existence of short range order, barriers of some form should exist. One of the objects of this investigation was to look for such barriers.

II. EXPERIMENTAL PROCEDURES

A. Material

A master alloy ingot was prepared from high purity silver (99.995 wt.%) and aluminum (99.995 wt.%). Weighed quantities of the pure metals were melted under argon in graphite crucibles by means of a high frequency induction technique and then chill-cast into copper molds. The ingot was then given a forty-eight hour homogenizing anneal at 550°C. The chemical analysis of the alloy is shown in Table I.

B. Specimen Preparation

Single crystal prismatic bars having the composition Ag 33 at.% Al and oriented such that the $\langle 1\bar{2}10 \rangle$ direction and normal to the $\{1\bar{1}00\}$ plane were at 45 ± 2° to the tensile axis were grown by the techniques previously described by Mote, et al.[1] Sections of the prismatic bar were then used as seed crystals from which single crystal strips with dimensions 10 × 3/4 × 0.025 in. were grown under argon. Finally, tensile specimens with dimensions 2.25 × 3/8 × 0.025 in. were spark cut from the single crystal strips. In order to remove the effects of spark cutting, the specimens were given a 15 min. anneal at 627°C then etched in a 40% nitric acid solution and finally electropolished to produce a smooth surface. After back reflection Laué x-ray photographs had been taken to confirm the initial orientation, the specimens were strained on an Instron Tensile Machine.

C. Testing Procedures

Special grips were designed to hold the specimen rigidly in place by two slide rods which screw into the upper grip and slide into the lower grip where they could be clamped by set screws. The entire grip unit is

then rigid and may be transferred to the tensile apparatus without introducing deformation prior to straining. High temperature tests were conducted with the specimen immersed in a constant temperature bath consisting of a molten mixture of sodium nitrate and sodium nitrite. Low temperature baths were either liquid nitrogen or liquid nitrogen-ethyl alcohol mixtures. Unless otherwise stated, all specimens were deformed at an unresolved strain rate of 10^{-2} per min.

Immediately after straining, the slip lines on the specimen were examined on a Zeiss Metallographic Microscope. Thin foils were then made by the window technique using the following electrolyte:

Potassium Cyanide	3.0 gm
Sodium Hydroxide	1.5 gm
Silver Cyanide	0.5 gm
Potassium Carbonate	0.3 gm
Distilled Water	100 gm

The polishing was carried out at temperatures slightly above the freezing temperature of the electrolyte ($\sim -5°C$). Optimum polishing conditions were obtained when using a potential of 3 volts and a current density of 0.02 amp/cm^2. All transmission electron microscopy observations were made with a Siemens Elmiskop electron microscope operated at 100KV and equipped with a Gatan double tilting stage.

D. Foil Orientation

Some limitations are imposed on the experiments due to problems arising from the electropolishing techniques. Most of the electrolytes tested during this investigation failed to polish surfaces which deviated more than 10 degrees from the basal plane. The electrolyte finally chosen was only of limited success in this regard. Consequently, as shown in Fig. 3,

most of the tensile specimens were so oriented that the large face was parallel to the basal plane. Although this particular orientation ensured a zero shear stress on the basal plane, it prevented a study of the dislocation distribution in all but (0001) sections. Moreover, in view of the particular symmetry of the (0001) orientation and the great many possible slip systems which can operate in hcp crystals, unambiguous Burgers vector determinations are impossible to achieve with the available low order reflections. The reflections necessary for an unambiguous Burgers are usually of higher order and are accessible only when the foil is in higher index orientations.

Therefore, a preliminary study was made of the reciprocal space in the vicinity of the [0001] reciprocal lattice section in order to gain the necessary familiarity of the regions containing these high index poles. The result of the preliminary investigation was the construction of a fully indexed [0001] Kikuchi map shown in Fig. 4. The map contains the poles of all the non-basal Burgers vectors commonly observed in hcp crystals. It, therefore, provides at a glance all the reflections necessary for an unambiguous Burgers vector determination which lie within 20 degrees of the [0001] orientation. Since tilting experiments were controlled by following the Kikuchi bands, the foil orientation was known at all times. More details of the construction and use of Kikuchi maps are described elsewhere.[5]

III. EXPERIMENTAL RESULTS

A. Stress-Strain Curves

Tensile tests were conducted at five different temperatures: 77°K, 210°K, 300°K, 400°K and 500°K. Fig. 5a shows the temperature dependence of typical tensile curves. Repeated yielding was observed at all temperatures except at 500°K. All crystals which deformed by repeated yielding exhibited a pronounced initial yield drop followed by a series of smaller drops occurring more or less at a constant average stress level. No apparent plastic flow was observed prior to the initial yield. At 500°K plastic flow became more uniform and a small amount of plastic flow occurred before the load reached its maximum value.

For comparative purposes the upper and lower critical resolved shear stresses were calculated for the most favorably oriented $\langle 1\bar{2}10 \rangle$ $\{1\bar{1}00\}$ slip system. The lower yield was arbitrarily taken to be the bottom of the initial yield drop. The values are in good agreement with those of Mote, et al.[1] and have been plotted on the curve taken from their work (see Fig. 2).

The repeated yielding phenomenon characteristic of dynamic strain aging has now been observed in single crystals of many fcc and bcc solid solutions of the noble metals. However, the only reported example of repeated yielding in single crystals of the ζ phases has been that of Thornton[6] who observed the effect in Cu 13.5 at.% Ge and Cu 16.5 at.% Ge. He found that, depending on both temperature and strain rate, repeated yielding can be replaced by homogeneous yielding. Repeated yielding has also been observed in polycrystalline Ag 33 at.% Al[7] but not in single crystals of the alloy. In the case of polycrystalline Ag 33 at.% Al, the

temperature dependence of the yield stress was practically the same as that for prismatic slip. However, the strain rate and temperature dependence of the repeated yielding was not investigated. Therefore, in order to obtain such information specimens were deformed at 77°K, 210°K and 300°K at four different unresolved strain rates from 10 $\dot{\epsilon}_o$ to 10^{-2} where $\dot{\epsilon}_o = 10^{-2}$ per min. Except for the case at 77°K and 10 $\dot{\epsilon}_o$ where fracture occured almost immediately, repeated yielding was observed for all strain rates. Although the load drops increased somewhat at the highest strain rate, the only apparent change was due to the reduction in time scale, i.e., the load peaks appeared closer together with increasing strain rate. (An example of the effect at 300°K is shown schematically in Fig. 5b). Since the repeated yielding phenomenon is independent of both strain rate and temperature, dynamical strain aging effects do not play an important role, as one might have expected, in view of the similarity in the effective volumes of silver and aluminum atoms.

B. Slip Line Patterns

Visual observations during the tensile tests showed that each load drop was associated with the appearance of a slip cluster across the gage section of the specimen. The initial clusters always occurred near one of the grips but they were soon followed by others at various points along the gage section. The surface under observation was parallel to the basal plane and, therefore, contained the primary $\langle 1\bar{2}10 \rangle$ slip direction. Consequently, the initial clusters were very faint and were observable only when viewed from certain critical angles.

With increasing total strain, a gradual transition occurred from a random formation of slip clusters to a preferential formation near already

existing ones, similar to slip band growth. This stage continued until the entire gage section was nearly covered by wide bands of slip clusters. Further slip beyond this stage apparently concentrates in one of the wide slip bands causing the specimen to begin literally slipping apart resulting in very large offsets at the edges of the specimen. (See Fig. 6a.) Secondary slip lines usually make their appearance at this time.

Tensile tests conducted at temperatures other than 300°K required the use of constant temperature baths so that visual observations could not be made during actual straining. However, metallographic examinations conducted immediately after the test showed that crystals deformed at 210°K and 400°K had slip trace patterns which were very similar to those obtained at 300°K. Figures 6a, b, c, and d are typical slip trace patterns after a 35% elongation at various temperatures. Specimens deformed at 500°K did not exhibit the coarse slip markings characteristic of repeated yielding. The slip traces were instead rather diffuse and somewhat wavy. Specimens deformed at 77°K were not examined optically but were electropolished immediately after straining in order to minimize possible recovery effects.

C. The Effect of Temperature and Strain on the Dislocation Distribution

The dislocation density in as grown crystals was too low to be measured accurately. Most of the areas examined showed only a few isolated dislocations but occasionally twist boundaries were observed. The upper limit of the dislocation density in as grown crystals was estimated by be approximately $10^8/cm^2$.

In the initial stages of deformation only a very few widely separated slip lines were observed. Thus, after electropolishing the chances of obtaining a suitable thin foil containing one of the slip bands were very small. Therefore, most of the observations to be reported in this section were taken from specimens deformed enough (~ 30%) to have developed reasonably wide bands, and thus increase the chances of observing portions of a slip band in thin foils.

The change in the dislocation distribution with temperature after 35% elongation is shown in Figs. 7 through 12 corresponding to 77°K, 210°K, 300°K, 400°K and 500°K respectively. Figure 7 is a low magnification micrograph of a typical area in a crystal deformed at 77°K. The most remarkable feature of the dislocation distribution is the very wide slip band. The band consists of many smaller clusters of very long and straight dislocations. Two sets of intersecting clusters are seen which lie parallel to the $\langle 1\bar{2}10 \rangle$ directions. Since the $\langle 1\bar{2}10 \rangle$ are slip directions, the clusters consist of screw dislocations. A particularly dense cluster has produced an offset in the wide slip band representing slip of several thousand Burgers vectors. The dark wide band in Fig. 7 actually contains a very high density of almost unresolvable prismatic loops. This can be more readily seen in Fig. 8 which is a higher magnification dark field micrograph of the edge of the dark band. Near the bottom of Fig. 8 where the deviation s from the Bragg condition is negative, the loops near the top surface produce very good strain contrast images.[8] Furthermore, the screw dislocations are in reality helices with extremely small pitch. The turns of the helices near the top surface also produce strong strain contrast images for example at A. Most of the helices in a cluster appear to be paired.

Figure 9a is a low magnification micrograph of a specimen deformed at 210°K. It corresponds to a region in the specimen whose surface slip pattern is shown in Fig. 6c. Figure 9b shows the same after 50% strain. The overall dislocation arrangement, particularly at higher total strains, is very similar to that obtained at 77°K. Here again the most prominent features are the high density of loops lying in well defined slip bands and long clusters of helical dislocations. Changes due to the increase in temperature appear to be one of scale rather than in distribution. The main changes are:

(a) At 210°K the slip bands were never as wide as those seen at 77°K but their number have greatly increased.

(b) At 210°K the density of the loops within a band appears to be somewhat smaller, while the average loop size appears somewhat larger than those observed at 77°K.

(c) At 210°K the number of long clusters have decreased relative to 77°K.

One of the most striking features of the dislocation distribution in Fig. 9a is its remarkable similarity to its surface slip pattern (see Fig. 6c). The slip associated with the slip bands undoubtedly produced the surface slip clusters which were seen to appear during each repeated yield drop. As was mentioned earlier, secondary slip was observed only in the later stages of deformation. Therefore, the offsets provide a very effective means of distinguishing the primary and secondary slip bands. In Fig. 9 the offsets show that the wide slip bands running from top to bottom correspond to the primary $\langle 1\bar{2}10 \rangle$ $\{1\bar{1}00\}$ slip system while narrow loop bands running horizontally represent secondary slip. In Fig. 6c, the coarse slip lines suffer the offsets and therefore, are associated with the wide slip

bands in Fig. 9, whereas the fine slip lines correspond to the narrow slip bands.

Figure 10 shows the dislocation distribution of the specimen shown in Fig. 6b. Again, the prominent features are the loop bands and long clusters of helical dislocations. The trend of the changes in dislocation distribution observed between 77°K and 210°K is continued up to 300°K. In fact, the loops are now large enough to be resolved as double arc loops.[9] There are fewer of the long clusters of helices and, in fact, many regions between slip bands were completely free of them. The helices again appear to be paired, and exhibit the abrupt change in background contrast characteristic of dipoles. A train of very steeply inclined dislocations is seen on the edge of each slip band in Fig. 10. Since the foil orientation is very near exact [0001] all the dislocations in the train are predominantly edge in character and are gliding on the primary $(1\bar{1}00)$ slip plane. As will be seen, such trains are always associated with slip bands.

Figure 11 shows a typical dislocation distribution in the specimen shown in Fig. 6d. Although loops are still clustered into bands, they and the helices no longer form in distinct regions, but rather intermingle with each other. Furthermore, the loops and the helical-turns are much larger. The loops are no longer equiaxed nor do they always exhibit double arc contrast. Many of the helices are intertwined which is suggestive of a probable mechanism of loop formation (see Section IV-C).

Figure 12 is representative of the dislocation distribution in a crystal deformed at 500°K. There has been a radical departure from the distribution characteristic of crystals deformed in regions I and II (see Fig. 1). None of the crystals deformed at 500°K contained the loop bands

or clusters of helical dislocations. Dislocations were always uniformly distributed and network formation such as the one at A were frequently observed. Networks are presumably formed by interactions between dislocations with different 1/3 $\langle 2\bar{1}\bar{1}0 \rangle$ Burgers vectors. This is confirmed by contrast experiments shown in Figs. 12b, c which were taken with different $\{20\bar{2}1\}$ reflections.

The effect of temperature on the dislocation distribution for constant total strains can be summarized as follows:

(a) Over regions I and II the changes in dislocation distribution is one of scale rather than in distribution. The high density of loops along slip bands and long clusters of helical dislocations remain as the most prominent features of the distribution throughout this temperature range.

(b) The density of the loops within a band decrease while the average size of the loop increases with increasing temperature.

(c) The density of the long clusters of helices decreases while the size of the helical turns increases with increasing temperature.

(d) In region III, the dislocations are uniformly distributed. The loops and clusters of helices are no longer observed.

The effect of increasing total strain on the dislocation distribution at 210°K is seen by comparing Figs. 9a and 9b, which correspond to 35% and 50% elongation respectively. As in the case of increasing temperature, the change is one of scale rather than distribution. The number of slip bands merely increase in number giving the appearance of slip band growth.

In fact, an increase in total strain appears to have the same effect as a decrease in temperature. The slip bands in Fig. 9b appear very similar to the wide slip band shown in Fig. 7. The same effect is seen at 300°K by comparing Figs. 10 and 13a.

D. The Effect of Specimen Shape on Dislocation Distribution

As mentioned earlier, the electrolyte was of only limited success in polishing foils with non-basal orientations. Figure 14 shows the dislocation distribution for one of the rare successes. The tensile orientation is shown in Fig. 14c. The primary $(1\bar{1}00)$ slip plane makes an angle of about 50° with the foil surface. The trace of this plane is almost horizontal in Fig. 14b, so that the cluster of helices appears as short steeply inclined dislocations. The loop bands are also observed. This shows that the particular distribution consisting of loop bands and clustering of helical dislocations does not depend on the shape of the tensile specimen. Figure 14a shows that basal cross slip occurs very frequently, a feature which was not seen in the surface slip line patterns of Fig. 3. This was due to the fact that in Fig. 3, the cross-slip plane was itself the surface under observation.

E. Burgers Vector Determinations

Figure 15a shows a slip band in a crystal strained 35% at 300°K. The foil orientation is near exact [0001] and the operating reflection is $g(2\bar{1}\bar{1}0)$. When the foil was tilted so as to bring the $g(20\bar{2}0)$ into operation, all the loops vanished as shown in Fig. 15b. According to the $\bar{g}\cdot\bar{b}$ criterion for dislocation extinction, the loops can have any one of the three following Burgers vector: $1/3[\bar{1}2\bar{1}0]$, $1/3[\bar{1}2\bar{1}3]$, or $1/3[1\bar{2}13]$. No

further information can be obtained from other reflections available in the [0001] orientation. The techniques used to overcome such ambiguities uses the fact that any Kikuchi band which passes through the zone axis of the Burgers vector satisfies the $\bar{g}\cdot\bar{b} = 0$ criterion for that particular Burgers vector. In order to eliminate the above ambiguity, the $\{20\bar{2}1\}$ Kikuchi bands were used since they pass through the $\langle 11\bar{2}0\rangle$ axes but not through those of the $\langle 11\bar{2}3\rangle$ directions. Other higher order reflections closer to the [0001] orientation (see Fig. 4) can be used but only at the expense of image quality.[5]

Such contrast experiments showed that all dislocations have Burgers vectors of the form $1/3\langle 11\bar{2}0\rangle$. For example, Fig. 16a, b and c have been correctly oriented with respect to the Kikuchi Map shown in d. The corresponding reflections and orientations are also indicated. Since the loops vanish for $g(20\bar{2}1)$ their Burgers vector is $b = 1/3[\bar{1}2\bar{1}0]$. On the other hand, the long helical dislocations and the train of steeply inclined dislocations vanish for $g(02\bar{2}1)$ so their Burgers vector is $b = 1/3[2\bar{1}\bar{1}0]$ which is parallel to the slip band. In fact, except for the loops, all dislocations in a cluster or slip band lying along a particular $\langle 11\bar{2}0\rangle$ direction were found to have the corresponding $1/3\langle 11\bar{2}0\rangle$ type Burgers vector. These include the steeply inclined dislocations within a slip band as seen, for example in Figs. 15 and 16b. Several of them are seen to have segments in screw orientation which have transformed into helical dislocations.

On the other hand, the vast majority of the loops within a slip band were found to have a $1/3\langle 11\bar{2}0\rangle$ type Burgers which was different from all other dislocations in the slip band. This was also found to be true in regions where duplex slip had occurred. For example, Fig. 17a shows two

intersecting slip bands in a crystal strained 45% at 210°K. Figure 17b shows that loops in both bands vanish for $g(20\bar{2}1)$. Therefore, their Burgers vector must be $1/3[\bar{1}2\bar{1}0]$ while all other dislocations in the intersecting slip bands have one of the other two equivalent $1/3\langle 11\bar{2}0\rangle$ Burgers vectors. Some loops do not vanish with the vast majority, as seen, for example, at A. Such loops, however, have been pinched off from screw dipoles and have the same Burgers vector as the parent dipole.

F. Dislocation Distribution Within a Slip Band

Figure 15b is an example of a relatively simple dislocation substructure within a slip band. Others with more complicated substructures are seen in Figs. 18b and 13b. Most of the steeply inclined dislocations appear to be all the same sign. Since their Burgers vectors are parallel to the slip band, they are predominantly edge in character, yet many have developed deep cusps usually seen only on screw dislocations. In this particular case the cusps could have been formed by interacting with one of the loops. Since the foil orientation for Figs. 13 and 18 is very near exact [0001], the projected width of most of the dislocations within a slip band is too large for the dislocation to be gliding on $\{1\bar{1}00\}$ planes. However, since the train of dislocations cut the foil surface along $\langle 1\bar{2}10\rangle$ directions their glide plane must be of the form $\{10\bar{1}\ell\}$. The glide plane is thought to be the $\{10\bar{1}1\}$ type since this assumption leads to reasonable estimates for the foil thickness, i.e., in the range of 3500Å to 4500Å. Unfortunately, dislocations were never observed to move, so that accurate measurements of the foil thickness could not be made.

As was mentioned earlier, trains of steeply inclined dislocations were usually seen near the edges of slip bands. However, we now see that many

others are found within slip bands. Moreover, the dislocations making up a train are all of the same sign. Such trains are never associated with the clusters of long helical dislocations. Therefore, the large offsets associated with slip bands, but not with the clusters are produced by the trains of steeply inclined dislocations. However, the fact that all slip bands also contain long helical dislocations strongly suggests that the clusters act as nuclei for slip bands.

G. Nature of the Prismatic Loops

The nature of the loops, i.e., whether vacancy or interstitial, was determined by the method Mazey, et al.[10] In order to ascertain the nature of the loop it is necessary to establish the sense of the Burgers vector relative to the operating reflection and the inclination of the plane of the loop relative to the electron beam. Using the convention of Bilby, et al.[11] as shown in Fig. 19, the positive direction of the loop is taken as clockwise when viewed from above. Defining s the deviation parameter as positive when the Kikuchi line lies outside the diffraction spot of the operating reflection, the image of the loop will lie outside the actual loop position when the product $(\bar{g}\cdot\bar{b})s$ is positive and vice versa. The inclination of the loop plane is determined by noting the change in size after large angle tilting under constant diffracting conditions.

Figures 20a, b and c are a series of micrographs of the same loop band shown in Figs. 13a and b. The corresponding reflections and orientations are shown in Fig. 20d. In Fig. 13b the loops vanish for $g(\bar{2}020)$ so that the loops have the Burgers vector $b = \pm 1/3[1\bar{2}10]$. Figures 20a and b show that the loops are in outside and inside contrast for $g(\bar{2}110)$ and $g(2\bar{1}\bar{1}0)$ respectively. Since s is positive for all micrographs the Burgers vector

of the loops must have the direction as indicated in Fig. 20.

In order to determine the inclination of the loop plane relative to the electron beam, the foil was tilted as shown in Fig. 20d about 15° along the $(2\bar{1}\bar{1}0)$ Kikuchi band to reach the $[0\bar{1}14]$ orientation. As shown in Figs. 20b and c, practically all the loops have increased in size. The sense of tilt is indicated in Fig. 20c. This can be easily shown by reference to Fig. 20d, Therefore, the sense of inclination of the loops when viewed along the tilt axis must be as shown in Fig. 21b. The two possible configurations for the loops are shown in Figs. 21c and d. The sign convention of Fig. 19 shows that Fig. 21c gives the correct sign of the Burgers vector and therefore, most of the loops shown in Fig. 20 are vacancy loops.

In most cases, loops observed in specimens deformed at temperatures lower than 300°K were less than about 200Å diameter, and are thus too small for the above techniques to be of value in determining their nature. In principle, it should be possible to uniquely determine the nature of small loops by strain contrast techniques.[12,13] However, when viewed under strain contrast conditions, the high density of loops within a slip band appear as a jumble of complex images. In many instances, it was possible to change the sense of the black-white image relative to the operating reflection for a given loop by changing any of a number of diffraction conditions. Consequently, it was not possible to determine uniquely the nature of loops in any of the slip bands observed at lower temperatures. The difficulties of such experiments are discussed in detail elsewhere.[13]

Some small loops were observed between slip bands. By contrast experiment, these were shown to exist only at the top surface of the foil and are, therefore, due to polishing and/or ion bombardment.[13] These loops are not

related to the damage in the slip bands and are irrelevant to this work.

IV. DISCUSSION

A. Metastable Arrangements

The principle features to be discussed are the broad slip bands containing a high density of perfect prismatic loops and the long clusters of helical dislocations which are characteristic distributions in specimens deformed in regions I and II (see Fig. 2).

The clusters of long helical dislocations have been shown to consist primarily of helical dipoles. Presumably they were initially screw dipoles which later transformed into helices by a mechanism and at a time which are, as yet, unknown. Prior to such a transformation, however, the clusters must have consisted primarily of screw dipoles. Such clusters could be formed by the operation of sources on neighboring glide planes.[14] If the distance between glide planes is y_o, then the screw part of the loops emitted by the sources will be unable to pass each other unless the applied stress exceeds $\mu b/4\pi y_o$. However, nearby screw dislocations of opposite sign tend to annihilate one another by cross slip. Whether such an event occurs depends critically on the distance separating the two dislocations and the crss of the cross slip plane. For the case of two screw dislocations of opposite sign gliding on neighboring prismatic planes, y_o apart, the force of attraction reaches a maximum when both lie on the same basal plane. Assuming that the screw dislocations are not extended, cross slip will occur only if the attractive stress $\tau \sim \mu b/2\pi y_o$ exceeds the crss for basal slip. If we use for Ag 33 at.% Al the values $\tau_B = 7\times10^8$ dynes/cm^2 (see Fig. 1), $\mu = 2.89\times10^{11}$ dynes/cm^2 (see ref. 3) and $b = 2.87\times10^{-8}$ cm, then cross slip will not occur unless y_o is less than about 200Å. The measured separation distance of most screw dipoles was found to lie between 500-200Å. As

expected, dipoles having separations on the order of 200Å were usually those in the process of pinching off loops. See, for example, the dipoles at A in Figs. 17a and 18a.

Consequently, screw dipoles need not always annihilate and if many sources operate over a small volume of crystal, clustering of screw dislocations can occur with the probability that most of the dislocations will be paired off as dipoles.[14] However, as pointed out by both Li[15] and Hazzledine[16], two or more screw dipoles are not stable and would tend to repel each other unless held in place by a large friction stress. Therefore, the consistent observations of such metastable clusters over a wide temperature range is in accord with the conclusions of Rosen, et al.,[3] that prismatic slip in Ag 33 at.% Al is controlled by the Peierls mechanism. Moreover, the fact that clusters are observed over both regions I and II suggests that the Peierls stress is still appreciable at room temperature. Thus, there appears to be some justification in the assumption made by Dorn and Rajnak[17] in their theory of the Peierls Mechanism, that the Peierls stress decreases only about linearly with increasing temperature. Although this assumption is inconsistent with the Kuhlman-Wilsdorf "uncertainty concept"[18] it now appears to have a strong basis in fact.

B. Formation of Slip Bands

The necessary barriers to slip proposed by Mote, et al.[1] have now been identified, namely the high density of loops within the slip bands. Theoretical calculations of Kroupa and Hirsch[19] have shown that loops can be very effective barriers to glide dislocations; and the direct observations of Price[20] have shown that in cadmium, a high density of loops can sufficiently harden a slip band so as to cause further slip to occur in undeformed

regions of a crystal. Therefore, the fact that prestrain does not reduce the crss for prismatic slip in region II, is no longer an effective argument against the Fisher mechanism.[21]

The alloy under investigation is known to be short range ordered[4] and the Fisher mechanism provides a natural explanation for the repeated yielding observed over regions I and II. Much of the work in disordering the crystal in the vicinity of the slip plane will be done by the first few dislocations. Therefore, the initial series of loops emitted by neighboring sources, which give rise to the long clusters of screw dislocations, could very well be responsible for the initial disordering. Further slip could then proceed in the same region at much lower stresses. Consequently, areas containing clusters represent "weak" regions in the crystal where further slip will most likely occur. Since the stress needed to produce the initial disordering is large, further slip will occur in bursts giving rise to a load drop and localized regions of intense slip, namely, the broad slip bands. Furthermore, such intense slip bursts are not blocked by usual barriers such as subgrain boundaries. (See for example Fig. 22).

The sequence of slip described above is consistent with the observation that large offsets as seen, for example, in Figs. 7 and 8, are produced by the broad slip bands, but not by the clusters of long screw dislocations. Such offsets must have been produced by the passage of many thousands of dislocations all having Burgers vectors of the same sign. Remnants of such dislocations were always observed in slip bands in the form of trains of steeply inclined dislocations and, thus, provided direct evidence for the slip burst phenomenon. Furthermore, such trains not only have the same Burgers vector as the clusters which precede it, but were also observed to

be gliding on the $\{10\bar{1}0\}$ plane or on one of its cross slip planes of the form $\{10l\ell\}$. Therefore, the sequence of slip also satisfies the conditions for maximum instability proposed by Washburn and Murty[22] to explain the repeated yielding phenomenon in pure copper.[23]

C. Formation of Loops and Helices

The vacancies required to account for the loops and helices are probably formed during plastic deformation by any one or combination of the many theoretical mechanisms described in the literature. However, since Ag 33 at.%.Al is an intermediate phase, one must also consider the possibility of vacancies originating from a defect lattice.

It is well known, for example, that beyond certain critical compositions many intermediate phases form vacancy concentrations well in excess of their thermal equilibrium value. On the basis of the theoretical work of Jones,[24] the critical composition in ζ-AgAl, if it exists at all, should occur at Ag 31 at.% Al. However, the lattice parameter measurements of Massalski and Cockayne[25] show that a sudden increase in the c/a ratio occurs at this composition and continues to increase as the aluminum rich phase boundary is approached. Such a change would not be expected if a defect lattice forms beyond the "critical" composition of Ag 31 at.% Al. Furthermore, if we were to assume that a defect lattice formed in spite of the increase in c/a, then in order to maintain the critical electron concentration per unit cell up to the composition Ag 33 at.% Al, a minimum vacancy concentration on the order of 10^{-2} is required. Since this concentration is about 100 times larger than the maximum theoretical concentration existing at the melting temperature for most metals, we can conclude that the vacancies in

Ag 33 at.% Al do not originate from a defect lattice.

On the other hand, experiments have shown that an unusually large number of point defects are created in specimens which deform by repeated yielding.[26,27] In these experiments, the rate of creation of vacancies is determined by measuring the decay rate of resistivity transients associated with load drops in crystals deforming by repeated yielding. According to Blewitt et al.,[26] the vacancy concentration produced during such load drops is given approximately by $C_V \sim 10^{-3}\epsilon$. For a total strain of 35%, the vacancy concentration is about 3×10^{-4}.

We can easily calculate the vacancy concentration needed to produce the high density of loops in a slip band from the equation:

$$C_V \sim \pi r^2 bn$$

where
r = average loop radius
b = Burgers vector of the loop
n = average loop density

If we take as an example the slip band of Fig. 12 corresponding to $\epsilon = 35\%$, and assume a foil thickness of 4500Å, we obtain a loop density on the order of 10^{15} loops/cm^3. This value is a lower limit since only regions where loops were actually countable were used in its evaluation. The average loop radius was found to be 125Å. Therefore, using the values $n \sim 10^{15}$, $r \sim 125$Å, $b \sim 3$Å, then $C_V \sim 2 \times 10^{-4}$ which agrees very well with the value calculated earlier.

Since the observed vacancy concentration is on the order of that obtained from relatively fast quenches, the vacancy condensation mechanism appears to be a very attractive one for explaining the presence of so many loops. In addition, the condensation mechanism could also account for the

presence of helices.

However, several experimental facts strongly suggest that loops are not formed by the above mechanism. First of all, we would expect the condensation mechanism to produce basal loops having one of the following Burgers vectors: [0001], 1/2[0001], or $1/6\langle 20\bar{2}3\rangle$. In contrast to this, the loops have been shown to be non-basal and their Burgers vector was unambiguously determined to be of the form $1/3\langle 2\bar{1}\bar{1}0\rangle$. In fact, except for sign, <u>all</u> loops had the <u>same</u> Burgers vector. Secondly, loops forming by a condensation of point defects would not favor a single Burgers vector over its two equivalent ones. Therefore, we can conclude that the loops probably do not form by point defect condensation, following a slip burst, unless the applied stress favors in some way, the formation of the observed perfect, non-basal loops all having the same Burgers vector.

Another possible mechanism is the formation of loops from helices. The extremely localized slip observed over regions I and II could easily produce more than enough point defects to transform the clusters of long screw dislocations into helices. The transformation could occur anytime during or after the tensile test. Since loops and helices were observed in specimens strained at 77°K where bulk diffusion is negligible, the helices would probably form after the test. However, bulk diffusion is not always necessary since Weertman[28] and deWit[29] have shown how helices can be formed at very low temperatures by pipe diffusion of vacancies. However, their mechanism is not believed to be important since it can occur only when the force on an initially straight dislocation satisfies very stringent conditions. Furthermore, their mechanism predicts that helices would transform preferentially from edge dislocations rather than from screw

dislocations which is exactly the opposite from what is observed.

A possible mechanism which accounts for both helices and loops is suggested in the following. Once a cluster of screw dipoles "weakens" the crystal sufficiently to trigger a slip burst, the point defects which are produced can turn the entire cluster into helical dipoles. If the separation of the original screw dipoles was sufficiently small, the corresponding helical dislocations could interact to produce loops. This would explain why, at constant total strains, the number of slip bands and clusters of helices decrease with increasing temperature and also why the size of the loops and helical turns increase with temperature. Yet, if loops were actually formed in this manner then they should have the same Burgers vector as the parent helical dipole. This is clearly not the case so that neither mechanisms of loop formation leads to the correct Burgers vector. Thus, the mechanism of formation of perfect loops in the slip bands remains unknown.

However, the loops do provide a natural explanation for the anomalous behavior of the crss for prismatic slip reported by other investigators.[1] Once a cluster initiates a slip burst, the slip band rapidly hardens due to the formations of loops. Further slip then occurs by slip band formation in undeformed regions of the crystal. Furthermore, the postulated slip sequence, i.e., clustering → slip burst → loop band formation, explains the repeated yielding and surface slip trace patterns observed in specimens deformed in regions I and II.

V. CONCLUSIONS

1. Single crystals of hexagonal ζ-Ag 33 at.% Al oriented for prismatic slip deformed by repeated yielding over regions I and II, while in region III plastic deformation occurs uniformly (Fig. 1).

2. Over regions I and II the most prominent features of the dislocation distribution were the high density of non-basal, perfect prismatic vacancy loops lying along well defined slip bands and the long clusters of helical dipoles. Both the slip bands and clusters lie parallel to the $\langle 1\bar{2}10 \rangle$ directions.

3. At constant total strain the density of the loops within a band decreases while their average size increases with increasing temperature.

4. At constant total strain, the number of the long clusters of helical dislocations decrease while the average size of the helical turns increase with increasing temperature.

5. In region III, the dislocations are uniformly distributed and the loops and clusters of helices are no longer observed.

6. At constant temperature, an increase in total strain produces an increase in the number of slip bands, but not in their loop densities.

7. The particular distribution consisting of loop bands and clusters of helices does not depend on the shape of the tensile specimen.

8. The slip bands can be correlated with surface slip lines, and the high loop density explains the anomalous behavior of the crss reported by other investigators. Once a slip band forms, it work hardens rapidly due to the presence of loops. Further slip then occurs by the formation of new bands in undeformed regions of the crystal. Therefore prestraining need not reduce the crss as expected from the Fisher mechanism.

9. All dislocations have a Burgers vector of the form $1/3\langle 1\bar{2}10\rangle$. Except for the loops, all dislocations in a cluster or slip band lying along a particular $\langle 11\bar{2}0\rangle$ direction have the corresponding $1/3\langle 11\bar{2}0\rangle$ type Burgers vector. The loops always have one of the other two equivalent Burgers vectors.

ACKNOWLEDGMENTS

The author is especially grateful to Professor G. Thomas for encouragement and support during his supervision of the research. Thanks are also due to Professor J. E. Dorn for valuable discussions and for making available the crystal growing equipment used during this investigation.

This research was supported by the U. S. Atomic Energy Commission and was completed under the tenure of a National Science Foundation Traineeship.

REFERENCES

1. J. D. Mote, K. Tanaka and J. E. Dorn, Trans. AIME, 221, 856 (1961).
2. A. Rosen, J. D. Mote and J. E. Dorn, Trans. AIME, 230, 1070 (1964).
3. E. Howard, W. Barmore, J. D. Mote and J. E. Dorn, Trans. AIME, 227, 1061 (1963).
4. J. P. Neumann, Acta Met., 10, 984 (1962).
5. P. R. Okamoto, E. Levine, and G. Thomas, J. Appl. Phys., in press, January 1967. See also E. Levine, W. L. Bell and G. Thomas, J. Appl. Phys., 37, 2141 (1966).
6. P. H. Thornton, Phil. Mag., 8, 2013 (1963).
7. K. Tanaka, and J. D. Mote, UCRL-9992 (1961).
8. W. L. Bell and G. Thomas, Phys. Stat. Sol., 12, 843 (1965).
9. W. L. Bell and G. Thomas, Phil. Mag., 13, 395 (1966). See also G. Thomas and W. L. Bell, Proc. Honolulu Conf. on Lattice Defects, Gorden and Breach, in press.
10. D. J. Mazey, R. S. Barnes and A. Howie, Phil. Mag., 7, 1861 (1962).
11. B. A. Bilby, R. Bullough and E. Smith, Proc. Roy. Soc., A231, 263 (1955).
12. M. F. Ashby and L. M. Brown, Phil. Mag., 8, 1063, 1649 (1963).
13. W. L. Bell, D. M. Maher and G. Thomas, Proc. Harwell Conf. on Small Clusters, H.M.S.O., in press (1966).
14. P. B. Hirsch and J. S. Lally, Phil. Mag., 12, 595 (1965).
15. J. C. M. Li, Discussions Faraday Soc., 38, 123 (1964).
16. P. M. Hazzledine, Discussion Faraday Soc., 38, 184 (1964).
17. J. E. Dorn and S. Rajnak, Trans. AIME, 230, 1052 (1964).
18. D. Kuhlman-Wilsdorf, Phys. Rev., 120, 773 (1960).

19. F. Kroupa and P. B. Hirsch, Discussion Faraday Soc., 38, 49 (1964).

20. P. B. Price, Electron Microscopy and Strength of Crystals, Eds. G. Thomas and J. Washburn, (Interscience, New York, 1963), p. 41.

21. J. C. Fisher, Acta Met., 2, 9 (1954).

22. J. Washburn and G. Murty, J. Appl. Phys., 37, 256 (1966).

23. Z. S. Basinski and P. J. Jackson, Phys. Stat. Sol., 9, 805 (1965).

24. H. Jones, Proc. Roy. Soc., A147, 396 (1934).

25. T. B. Massalski and B. Cockayne, Acta Met., 7, 762 (1959).

26. T. H. Blewitt, R. P. Coltman and J. K. Redman, Report of the 1954 Conference on Defects in Crystalline Solids, Phys. Soc., London, 369 (1953).

27. J. M. Anderson and A. F. Brown, Phys. Stat. Sol., 12, 309 (1965).

28. J. Weertman, Trans. AIME, 227, 1439 (1963).

29. R. deWit, Trans. AIME, 227, 1443 (1963).

Table I

Chemical Composition in Weight Percent

Mark	Top	Middle	Bottom
Ag	88.95	88.89	88.92
Mg	0.001*	0.001	0.001
Cu	0.002	0.003	0.002
Ca	---	0.001*	---
Ni	0.001*	0.001*	0.001*
Cr	0.001	0.001	0.001
Fe	0.002	0.002	0.002
Al	Bal	Bal	Bal

*Indicates less than

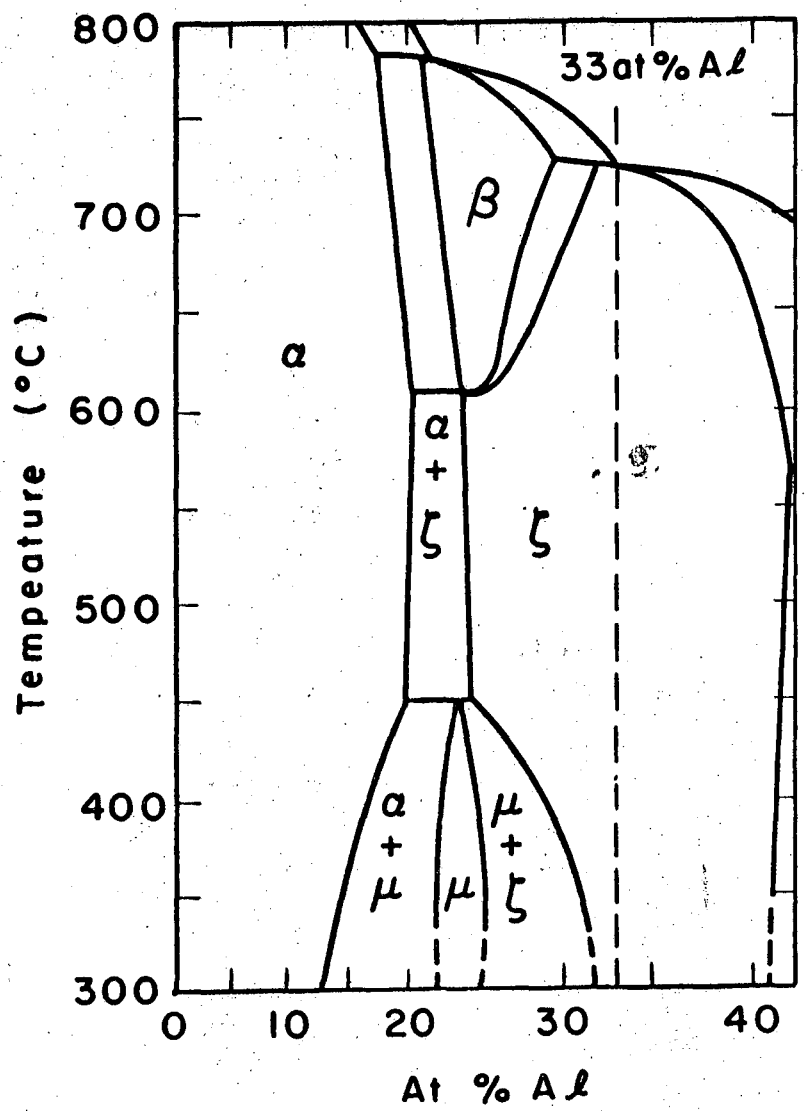

MUB 13665

Fig. 1 The silver-rich portion of the silver-aluminum equilibrium diagram (after Hanson).

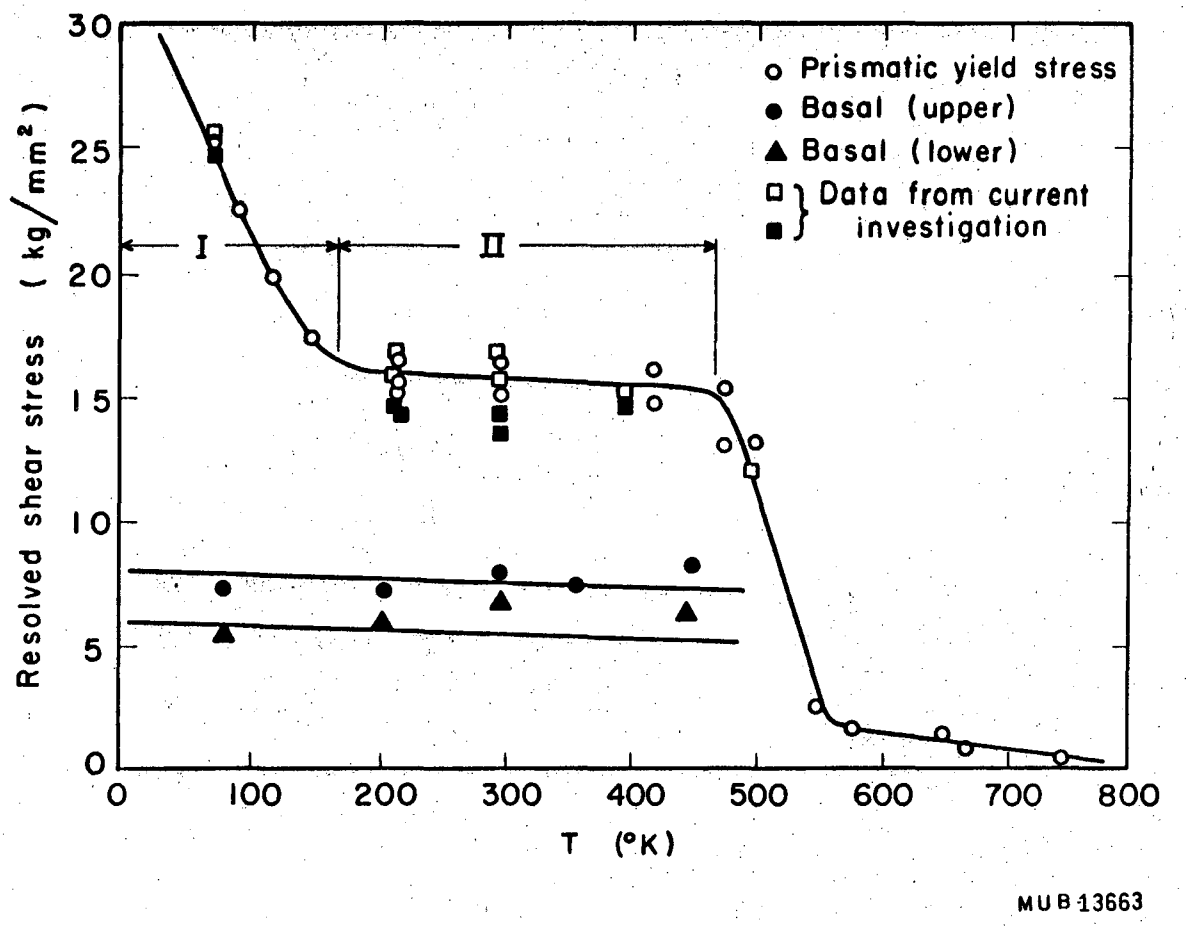

Fig. 2 Effect of temperature on the critical resolved shear stress for prismatic and basal slip (after Mote[1]). Squares indicate values obtained during the present investigation.

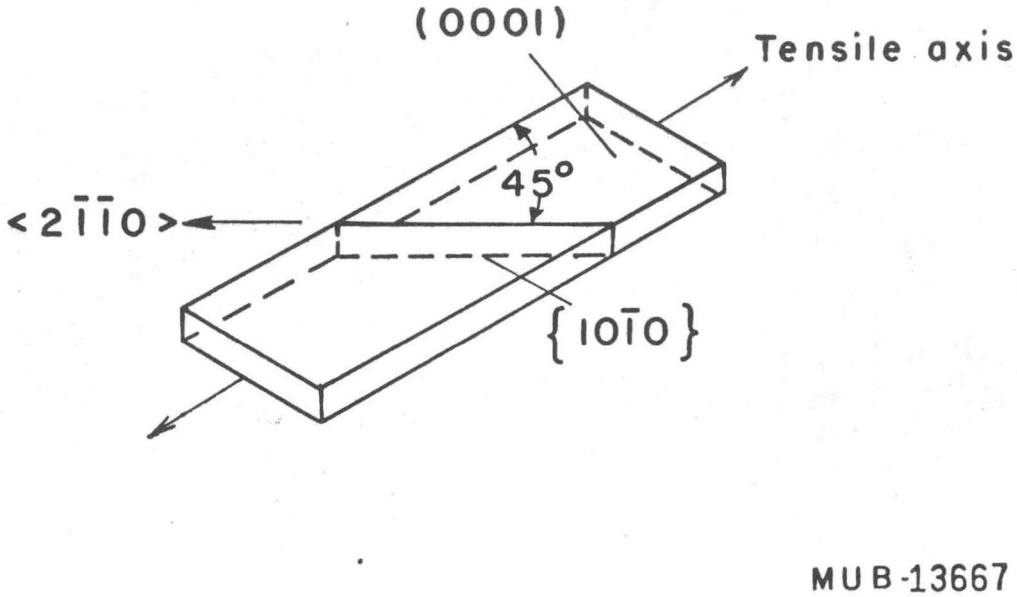

Fig. 3 Specimen tensile orientation.

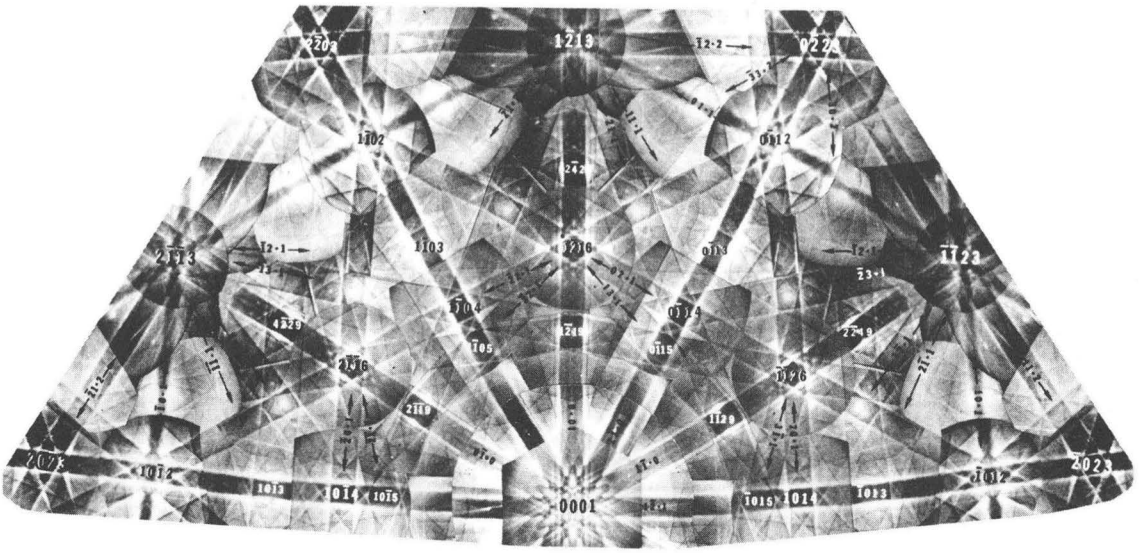

XBH671 3

Fig. 4 Composite Kikuchi map obtained from single crystals of h.c.p. Ag 33 at.% Al (c/a = 1.588). The map includes all reciprocal lattice sections and Kikuchi bands lying within 35° of the [0001] zone axis.

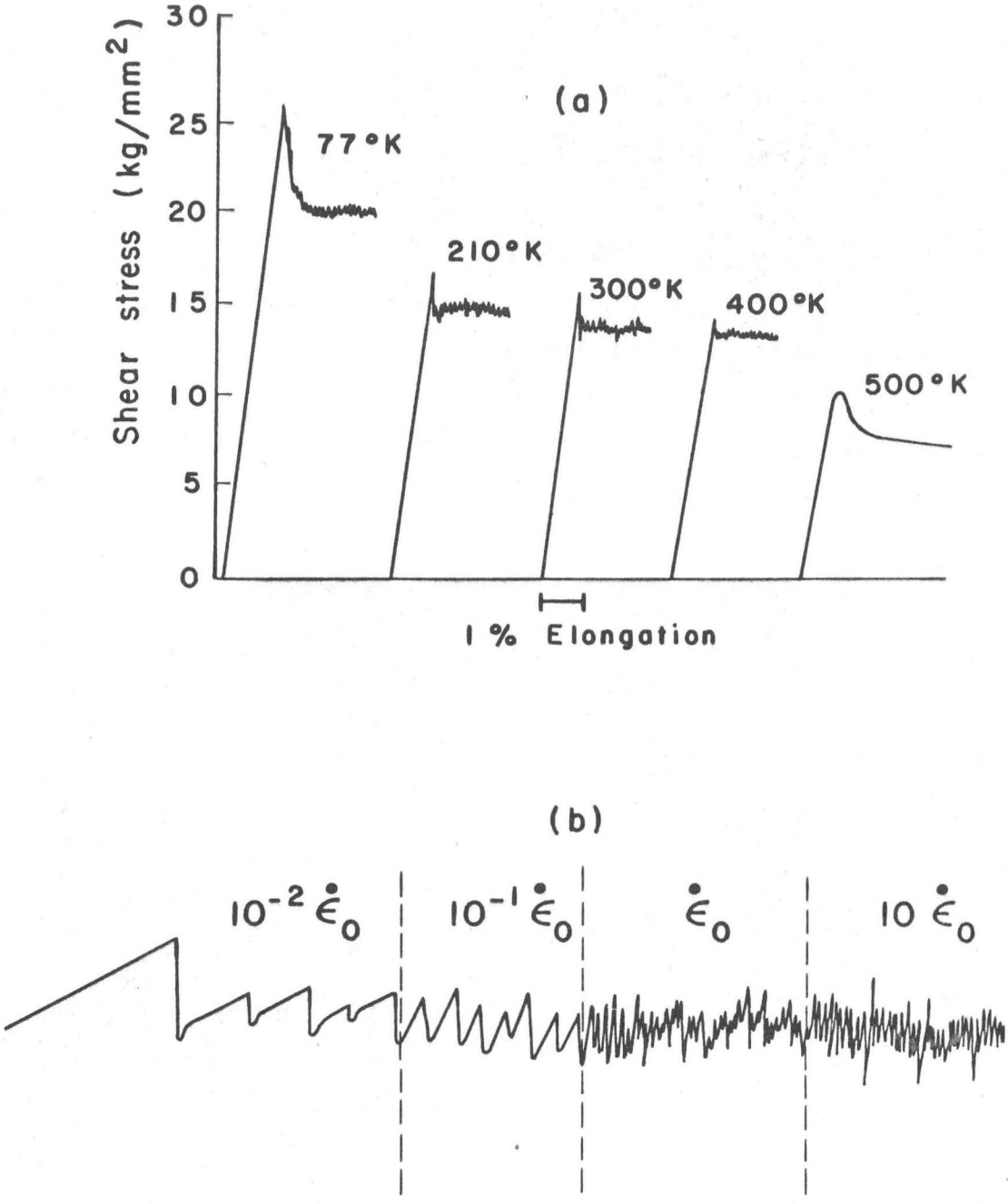

MUB 13664

Fig. 5 (a) Effect of test temperature on the form of tensile curves (schematic).

(b) Effect of unresolved strain rate on the form of the tensile curve at 300°K. $\dot{\epsilon}_o = 10^{-2}$ per min. (schematic).

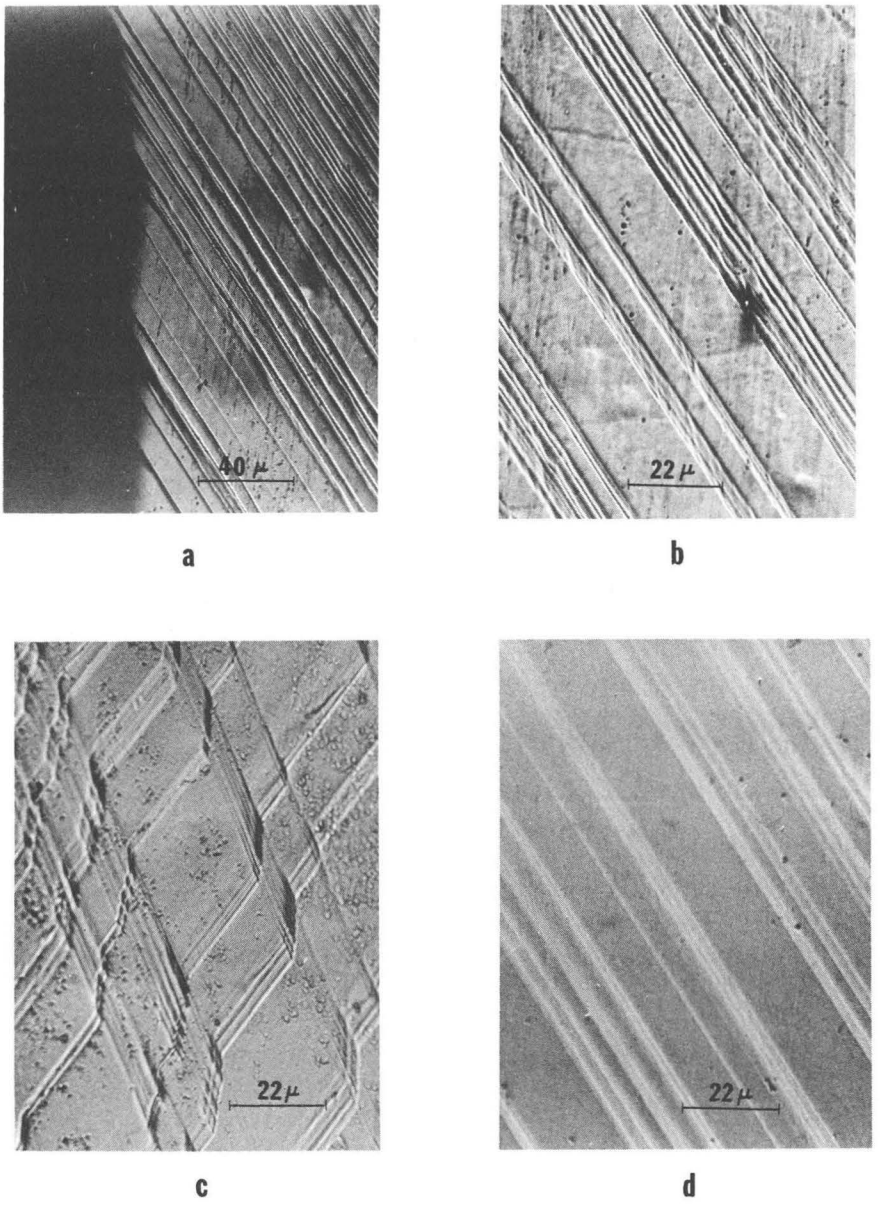

ZN-6041

Fig. 6 Typical slip line patterns on (0001) surfaces of crystals strained 35% at

(a) T = 300°K (×150)

(b) T = 300°K (×500) same specimen as in (a)

(c) T = 210°K (×500)

(d) T = 400°K (×500)

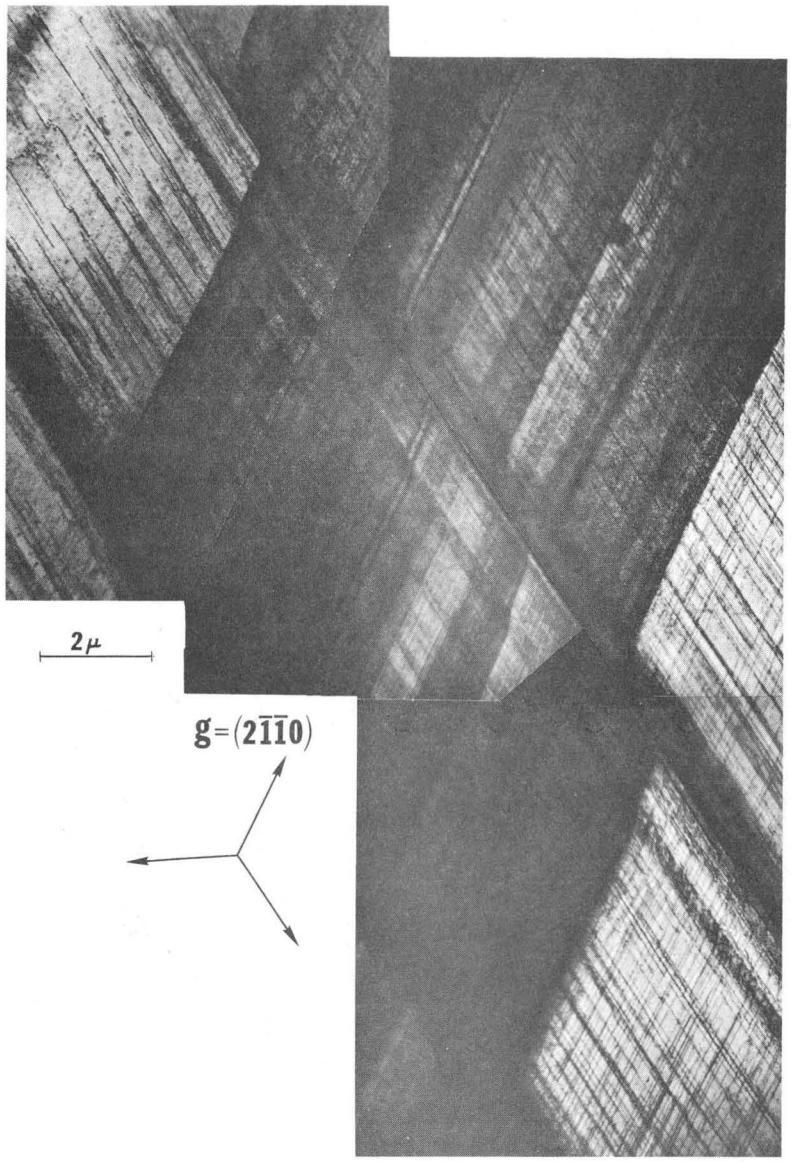

ZN-6042

Fig. 7 Typical dislocation distribution at T = 77°K, ϵ = 35% foil orientation: [0001]. The slip band consists of a high density of unresolved prismatic loops.

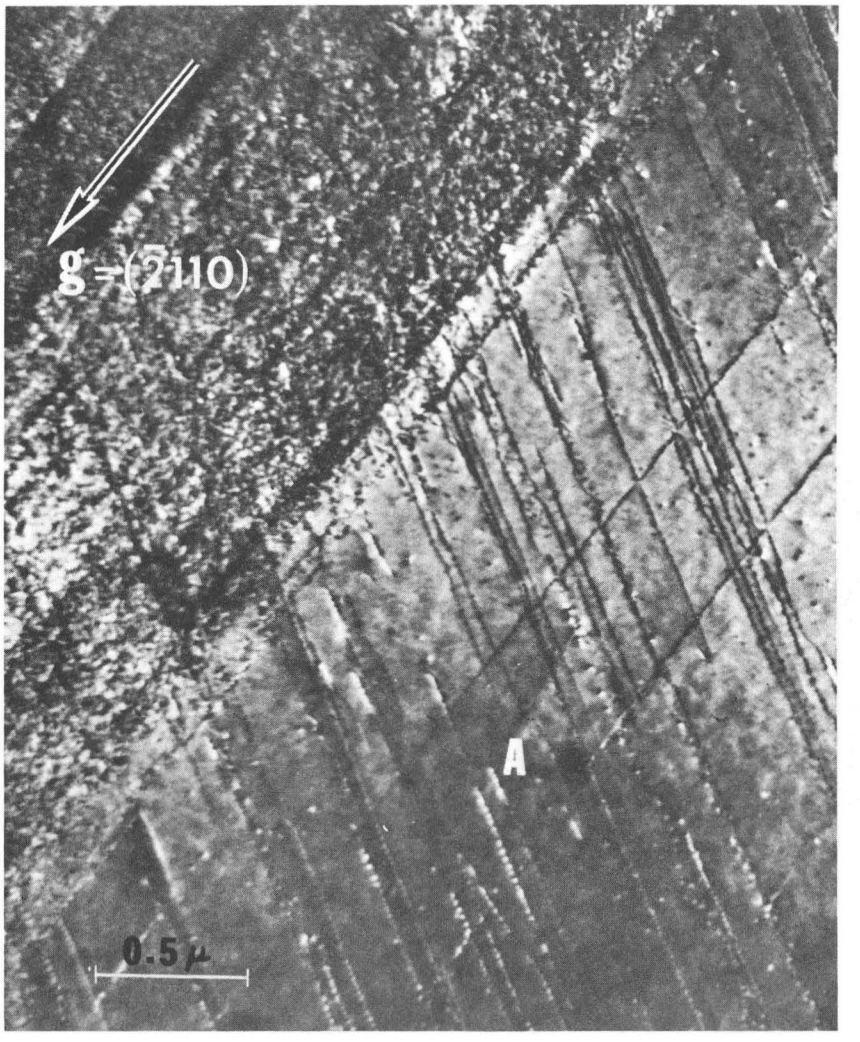

ZN 6043A

Fig. 8 Dark field micrograph of the edge of the slip band in Fig. 7. Note the black-white strain contrast images of the turns on helical dislocations at A. Note also the clustering of helices.

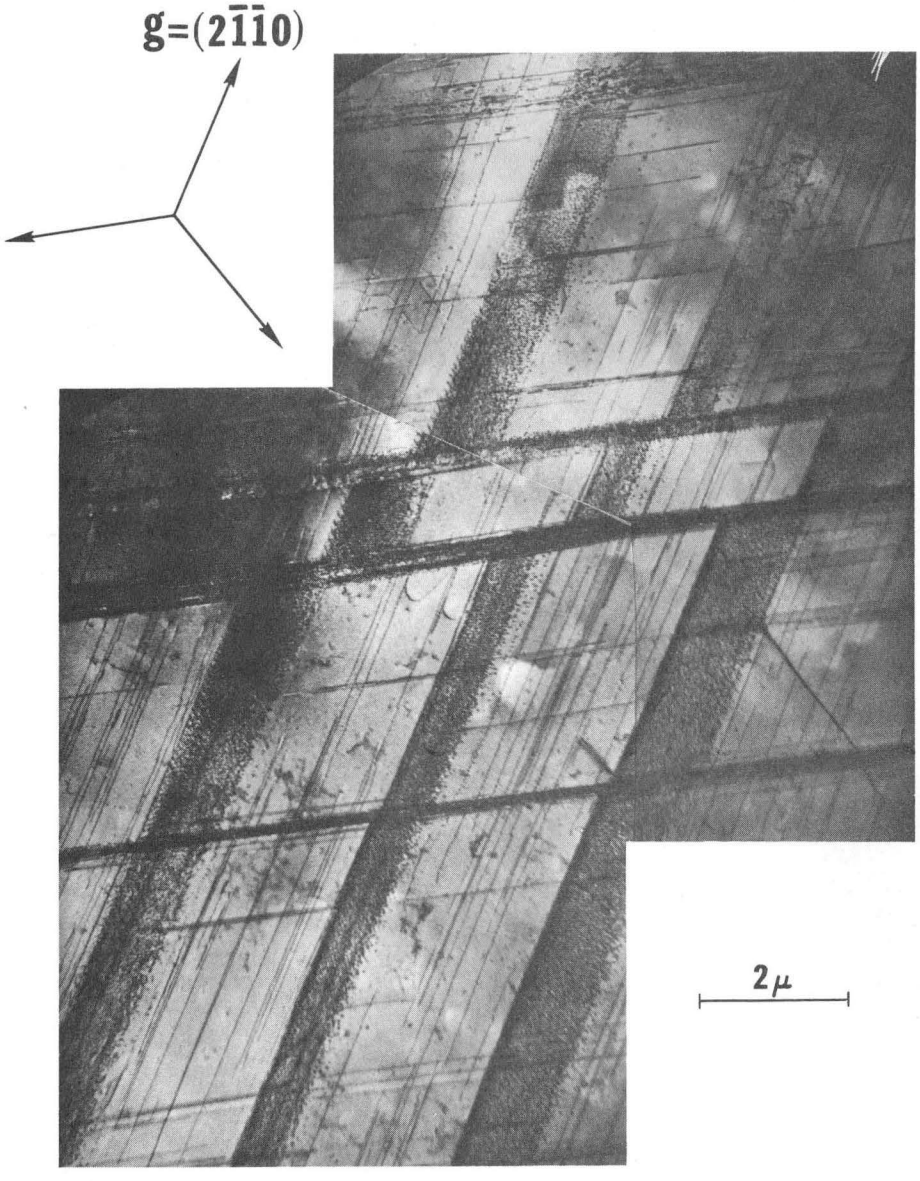

(a)

ZN-6044

Fig. 9a Typical dislocation distribution at T = 210°K, ϵ = 35% foil orientation: [0001]. Note offsets on primary slip bands and clustering of long helical dislocations between bands. Compare to Fig. 6c.

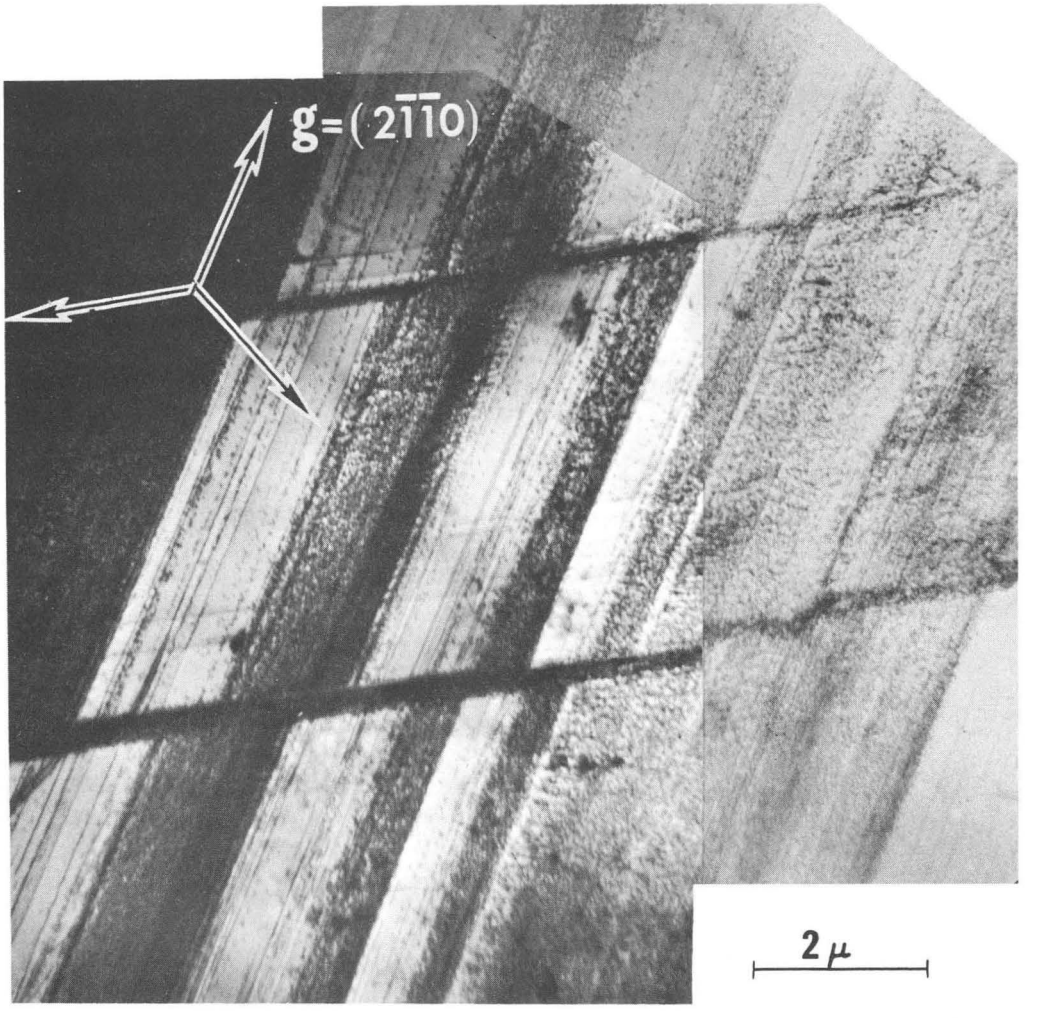

(b)

ZN-6045

Fig. 9b Typical dislocation distribution at T = 210°K, ϵ = 50%. Foil orientation: [0001]. Note the increase in the number of slip bands. The overall distribution appears similar to that in Fig. 7.

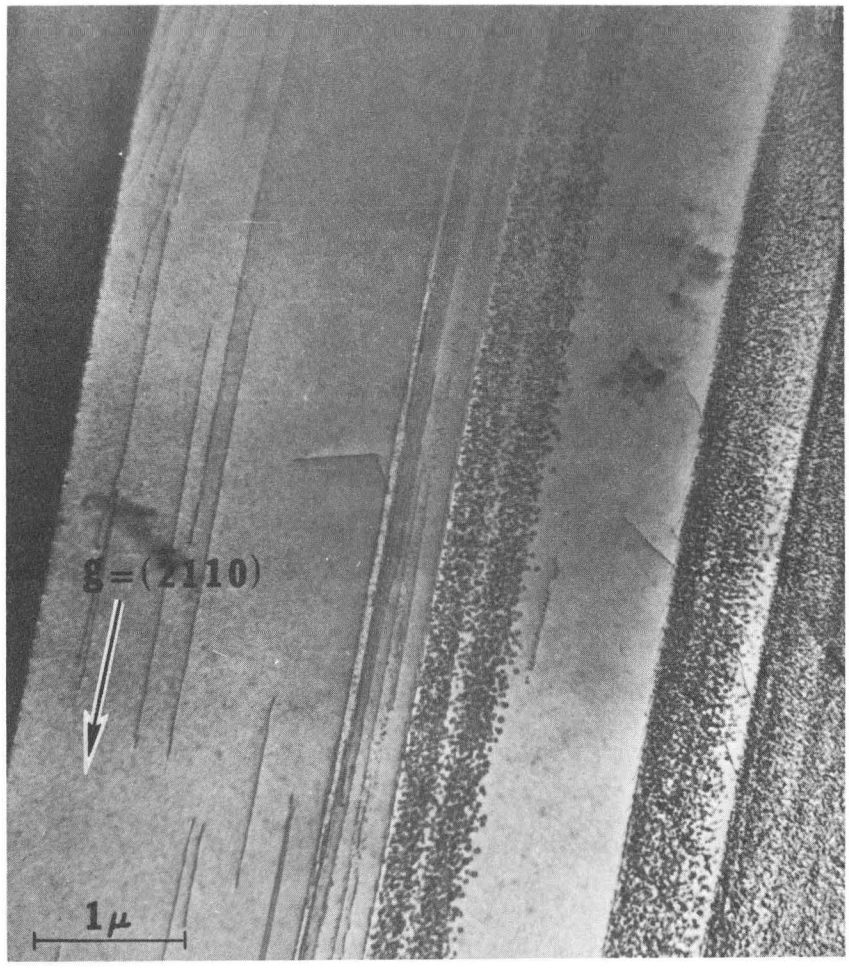

ZN 6046A

Fig. 10 Typical dislocation distribution at T = 300°K, ϵ = 35% foil orientation: [0001]. Note the high density of double-arc loops.

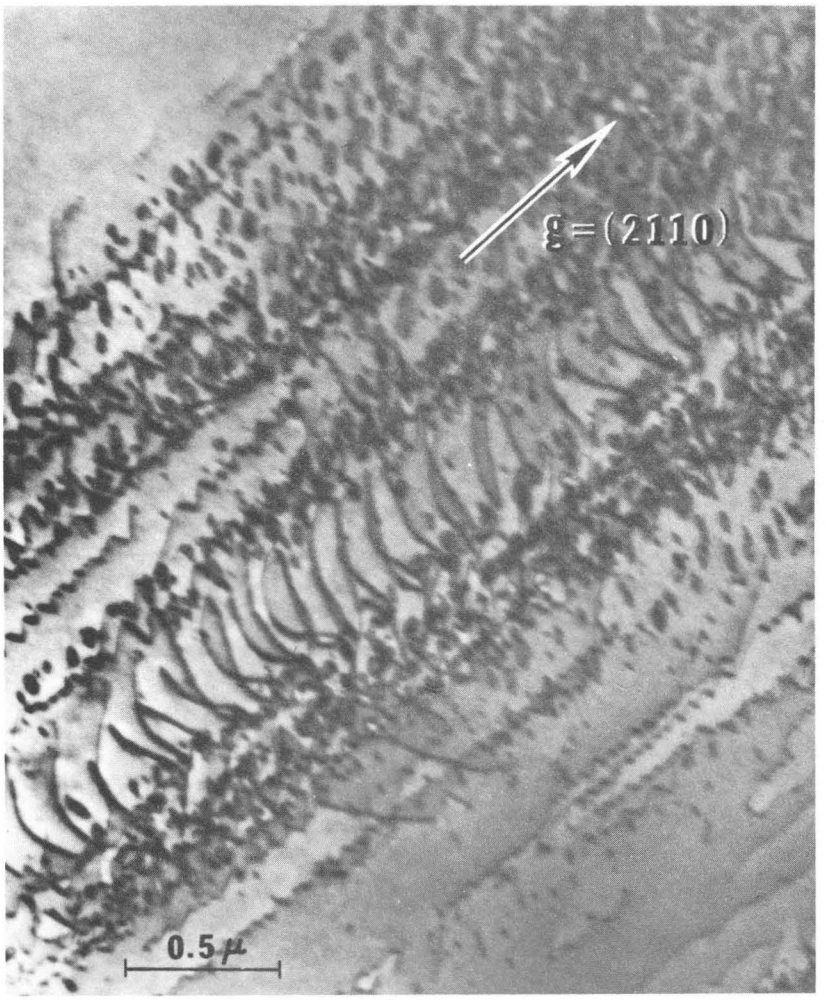

ZN 6047A

Fig. 11 Typical dislocation distribution at T = 400°K, ϵ = 35%
foil orientation: [0001].

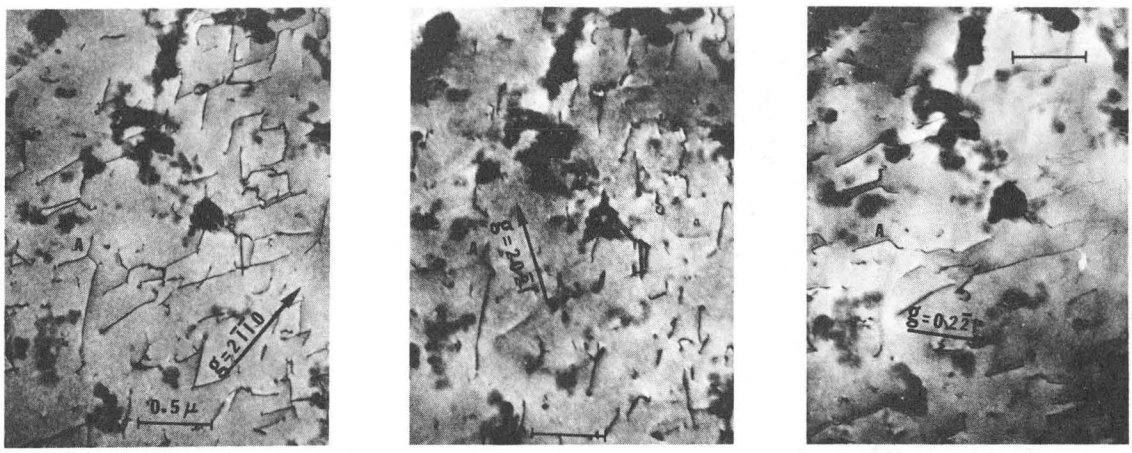

(a) (b) (c)

ZN-6048

Fig. 12 (a) Typical dislocation distribution at T = 500°K, ϵ = 35%, foil orientation: near $[0\bar{1}13]$(see Fig. 4) g = $(2\bar{1}\bar{1}0)$

(b) Same area with secondary dislocations out of contrast, foil orientation: ~8° off $[0\bar{1}13]$ towards $[\bar{1}\bar{1}23]$ g = $(20\bar{2}1)$.

(c) Same area with primary dislocations out of contrast, foil orientation: near $[0\bar{1}14]$ (See Fig. 4) g = $(02\bar{2}1)$.

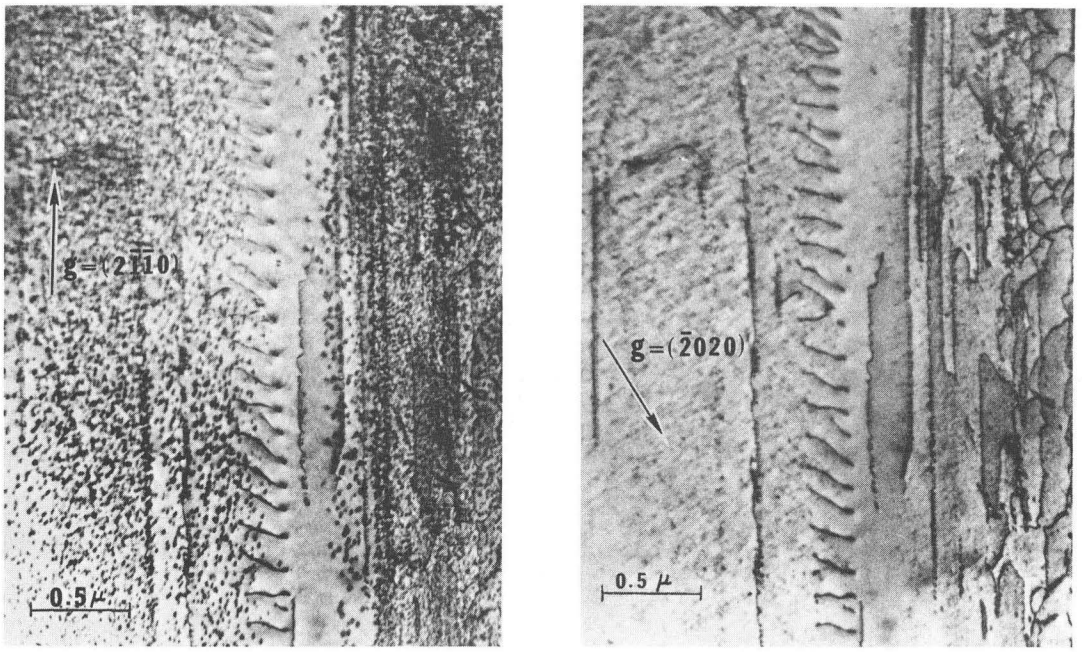

(a) (b)

ZN-6049

Fig. 13 (a) Typical loop band T = 300°K, ϵ = 35% foil orientation: [0001], g = (2$\bar{1}\bar{1}$0). (b) Note same area with loops out of contrast for g = ($\bar{2}$020). Note heavily cusped dislocation at right.

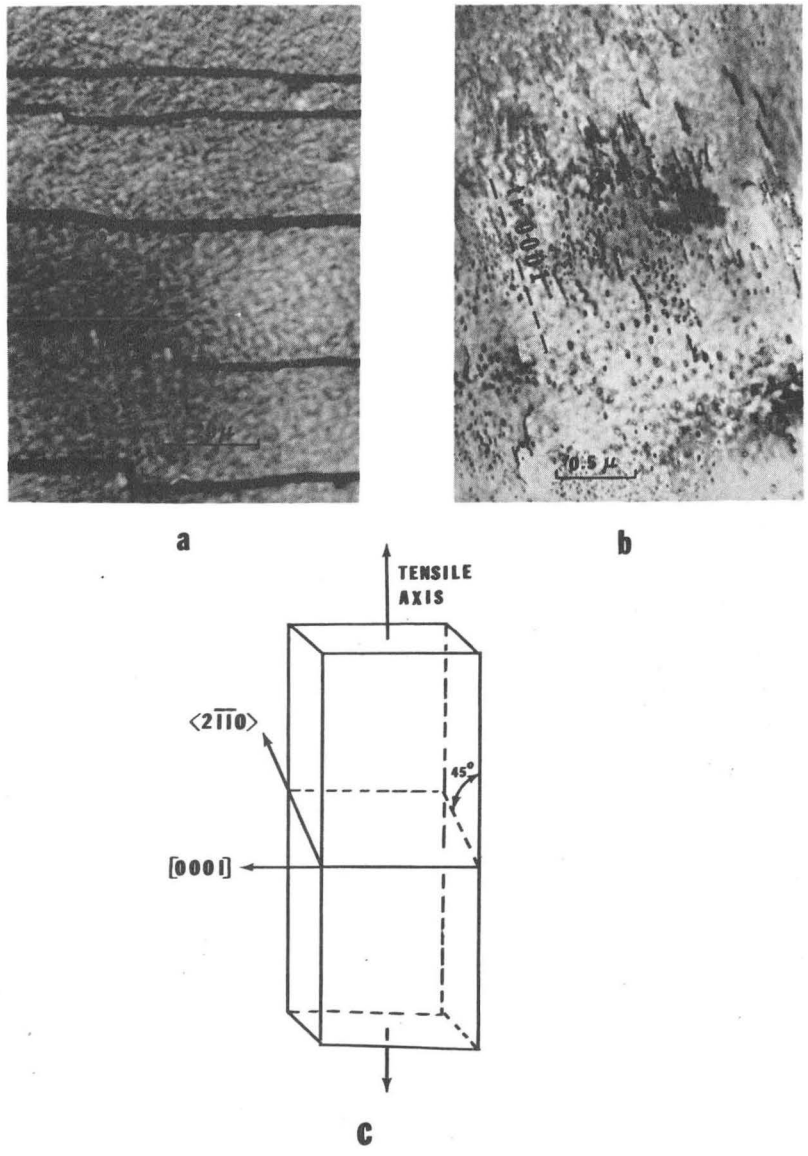

ZN-6050

Fig. 14 (a) Typical slip pattern on irrational face of specimen strained 20% at 300°K. Note frequent cross slip onto basal planes.

(b) Typical substructure from specimen shown in (a). Note loops and helices. Primary {1$\bar{1}$00} slip plane is inclined about 50° to foil surface.

(c) Orientation of the tensile specimen shown in (a) and (b).

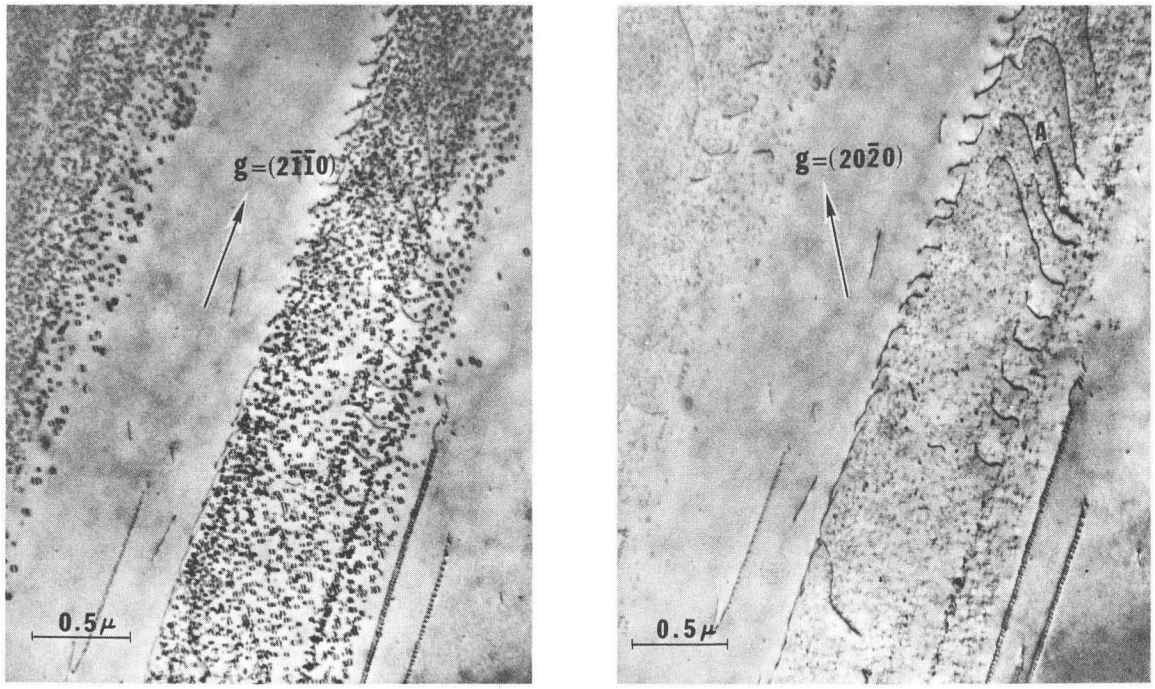

(a) (b)

ZN-6051

Fig. 15 (a) Typical slip band at T = 300°K, ϵ = 35% foil orientation: [0001].

(b) Same slip band with loops out of contrast for g = (20$\bar{2}$0). Note inclined dislocations with segments in screw orientation which have transformed to helices.

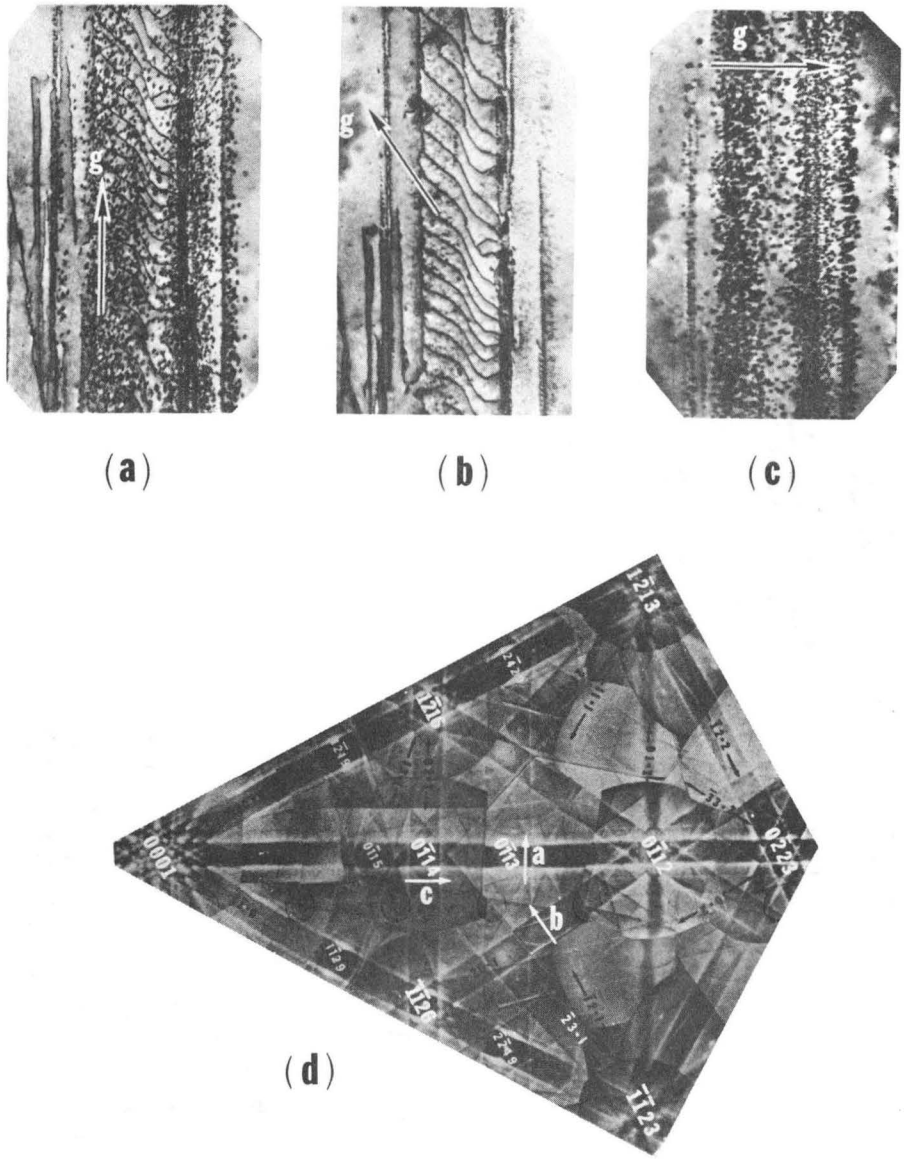

XBH671 2

Fig. 16 Illustrating the application of the Kikuchi map for Burgers vector determinations in deformed Ag 33 at.% Al. The micrographs are correctly oriented with respect to the map on which foil orientation and operating reflections are indicated. (a) Bright field micrograph of a slip band observed at 300°K after 35% strain. The operating reflection is $g(2\bar{1}\bar{1}0)$ so all dislocations with $1/3\ \langle 2\bar{1}\bar{1}0\rangle$ Burgers vector are in contrast. (b) All loops vanish for $g(20\bar{2}0)$ thus they have the Burgers vector $\bar{b} = 1/3\ [1\bar{2}10]$. (c) All dislocations except the loops vanish for $g(02\bar{2}1)$ so that they have the Burgers vector $\bar{b} = 1/3\ [2\bar{1}\bar{1}0]$.

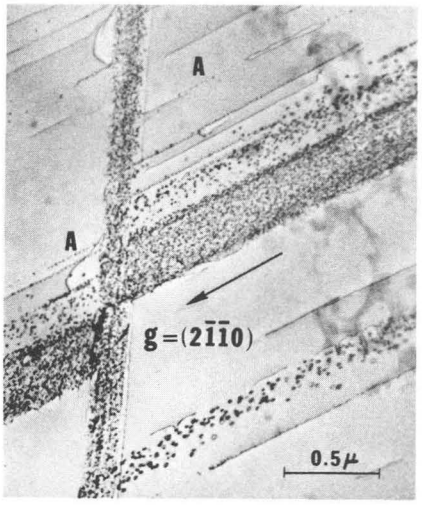

(a)

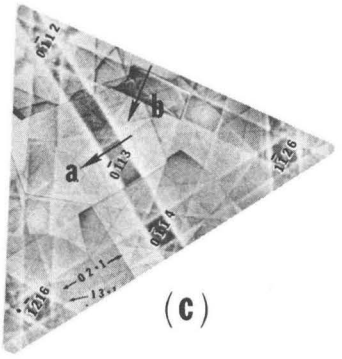

(c)

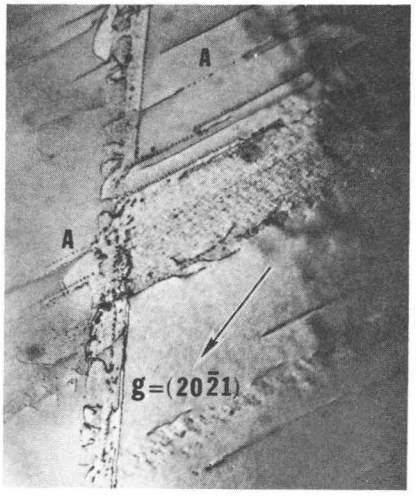

(b)

ZN-6052

Fig. 17 (a) Intersecting loop bands: T = 210°K, ϵ = 45% foil orientation: [0$\bar{1}$13] Note row of loops at A being pinched off a screw dipole.

(b) Same area showing loops in both bands out of contrast for $\bar{g}$ = ($\bar{2}$201). Note loops at A have not vanished.

(a)

(b)

ZN-6053

Fig. 18 (a) Typical loop band at T = 210°K, ϵ = 45%
foil orientation: (0001).

(b) Same loop band with loops out of contrast.
Note cusped dislocation gliding on {10$\bar{1}$1} planes.

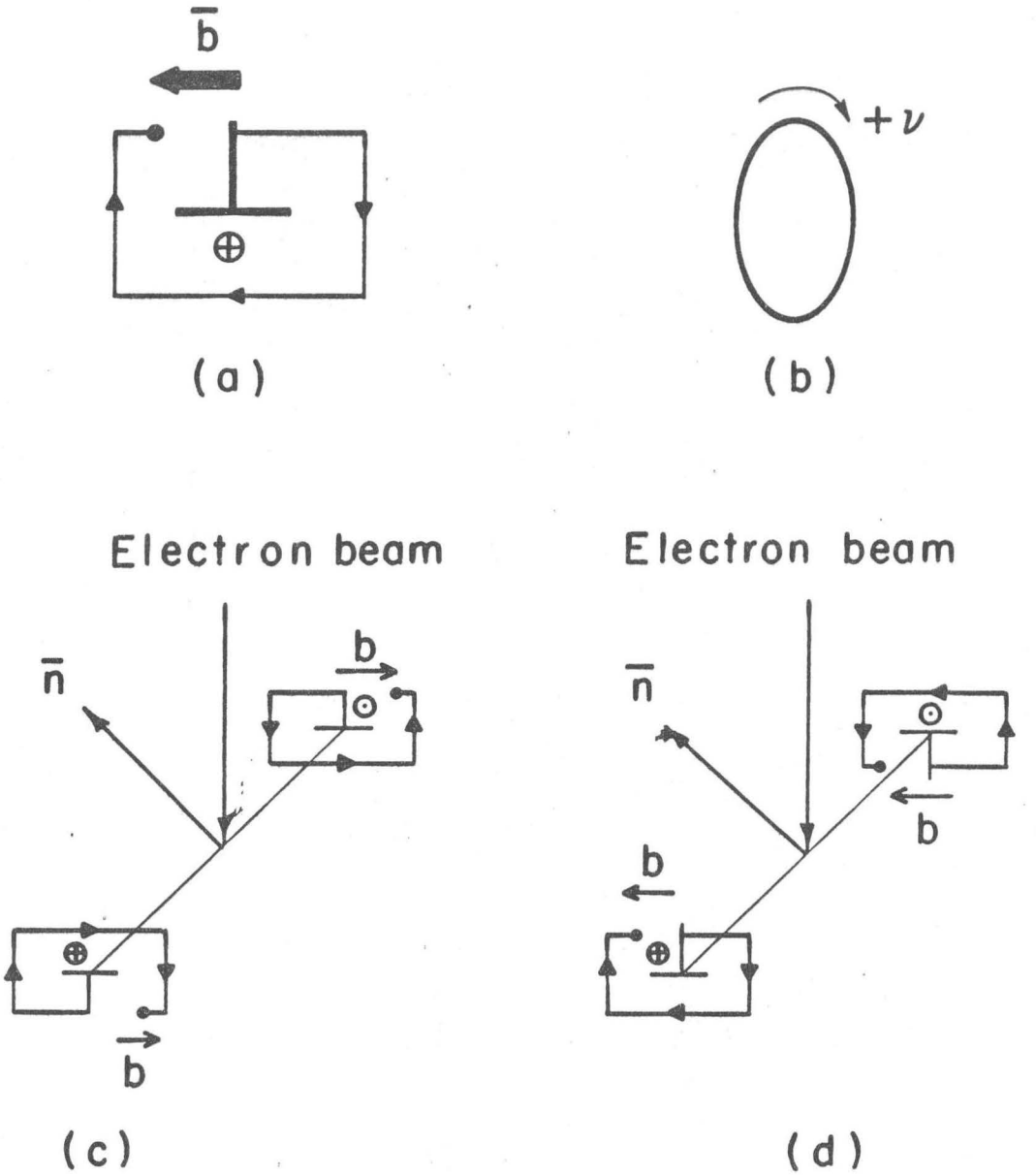

MUB 13666

Fig. 19 (a) Sign convention for defining the sense of the Burgers vector.

(b) Convention for defining the positive direction around loops as viewed on the screen.

(c) Cross-sectional view of vacancy loop.

(d) Cross-sectional view of interstitial loop. After Mazey, et al.[10]

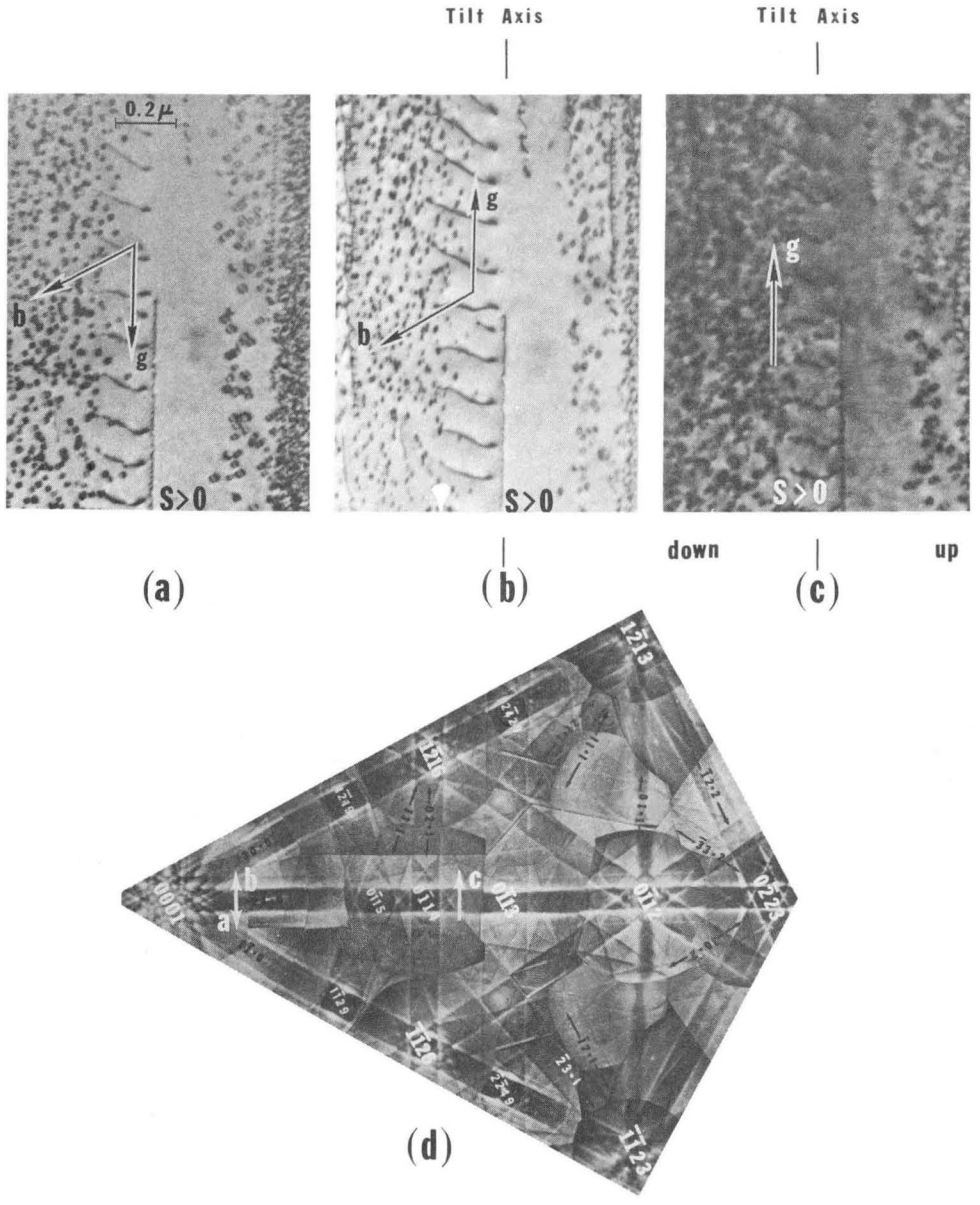

ZN-6054

Fig. 20 (a) and (b) showing the sense of the Burgers vector of the loops.

(c) After tilting approximately 15°. Note loops increase in size.

(d) Kikuchi map indicates the reflections used and direction and sense of tilt.

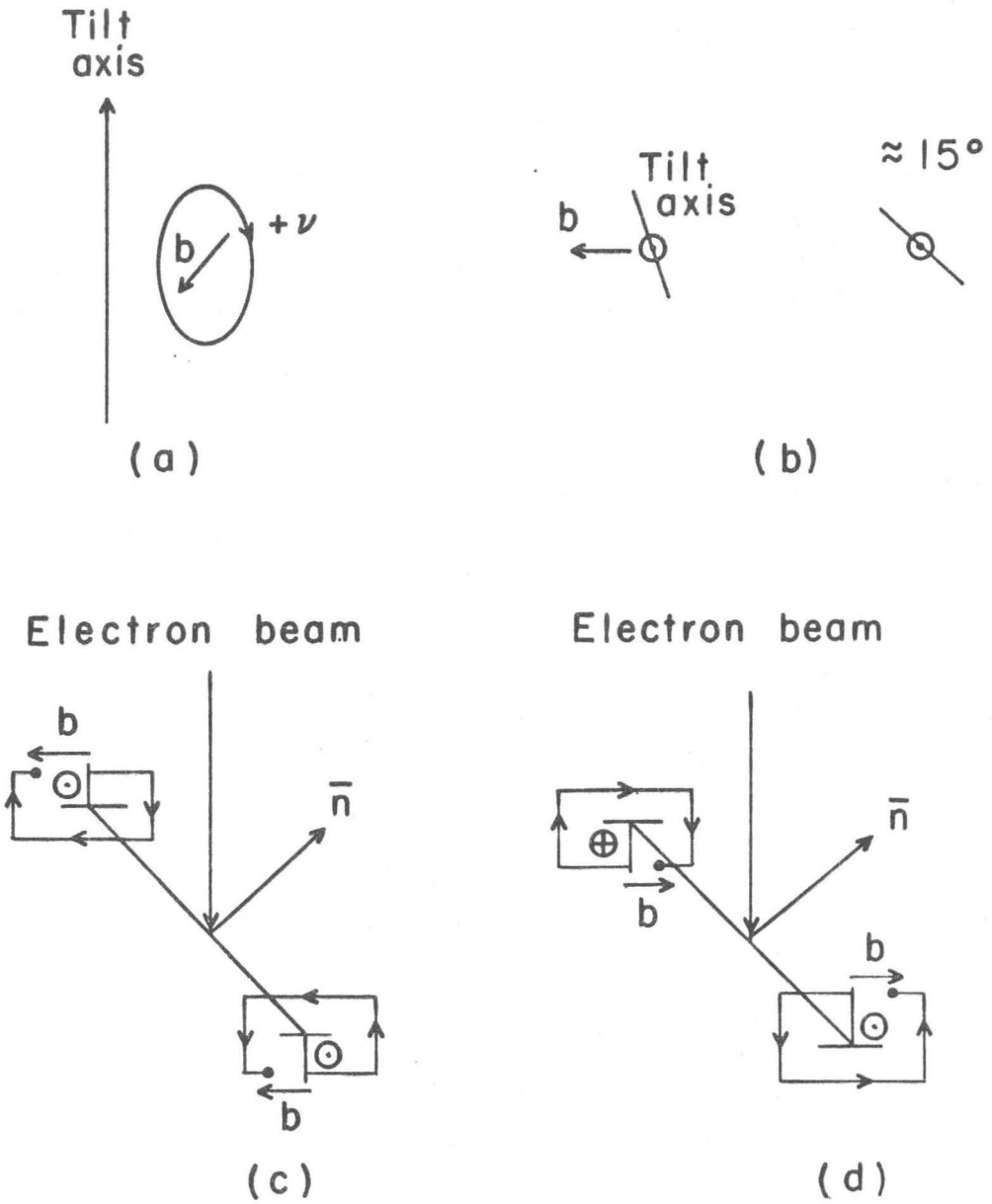

MUB-13662

Fig. 21 Possible configurations for loops in Fig. 20. Application of sign convention shows that (c) gives the correct sign of the Burgers vector.

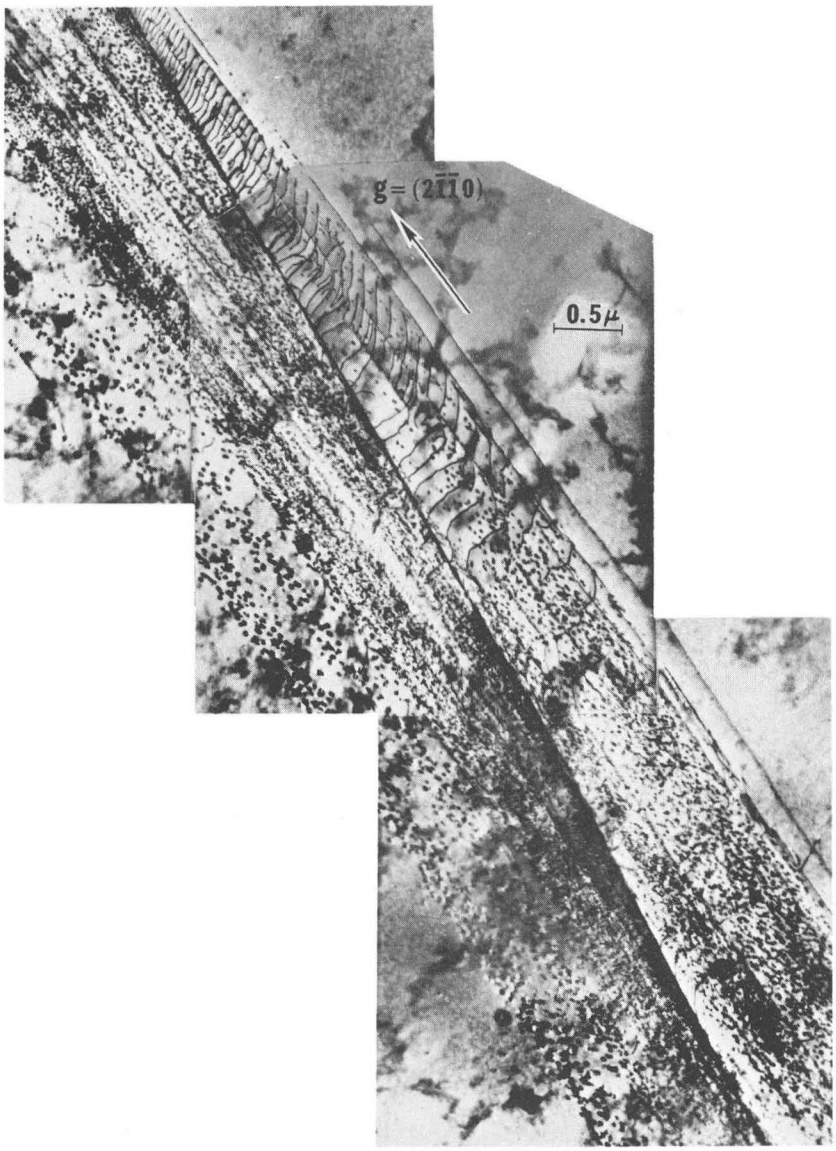

ZN-6055

Fig. 22 Shows a slip band penetrating across a subgrain boundary. g = (2$\bar{1}\bar{1}$0).

This report was prepared as an account of Government sponsored work. Neither the United States, nor the Commission, nor any person acting on behalf of the Commission:

A. Makes any warranty or representation, expressed or implied, with respect to the accuracy, completeness, or usefulness of the information contained in this report, or that the use of any information, apparatus, method, or process disclosed in this report may not infringe privately owned rights; or

B. Assumes any liabilities with respect to the use of, or for damages resulting from the use of any information, apparatus, method, or process disclosed in this report.

As used in the above, "person acting on behalf of the Commission" includes any employee or contractor of the Commission, or employee of such contractor, to the extent that such employee or contractor of the Commission, or employee of such contractor prepares, disseminates, or provides access to, any information pursuant to his employment or contract with the Commission, or his employment with such contractor.